Christian-Albrechts-Universität zu Kiel

Mathematisch-Naturwissenschaftliche Fakultät

Universität Bremen

Modelling and Retrieval of Sea Ice Thickness from Microwave Radiometer Satellite Observations

Thesis

Master of Science Programme

Climate Physics: Meteorology and Physical Oceanography

by

Justus Heilingbrunner

1108877

Advisor: Prof. Dr. Arne Biastoch

Co-Advisor: Dr. Gunnar Spreen

Kiel, April, 2023

Abstract

Sea ice extent in the Arctic Ocean has been declining since continuous satellite measurements of sea ice extent began in 1978. The proportion of thick multi-year sea ice in the Arctic that is at least 5 years old decreased from 30 % to 2 % between 1979 and 2018, and the proportion of thin first-year sea ice increased from about 40 % to 60-70 % over the same period. Thin sea ice is one of the key parameters characterizing and influencing the Earth's climate and ocean-atmosphere heat exchange in the polar oceans, so its accurate representation is important.

With brightness temperatures and retrieval algorithms, the sea ice thickness is measured on a large scale by satellites with passive microwave radiometry at 1.4 GHz (L-band), such as SMOS or SMAP, providing continuous all-weather coverage of the SIT at different spatial resolutions over the Arctic and Antarctic. The CIMR mission, to be launched in 2029, will also continue L-band observations. A new sea ice thickness retrieval algorithm has been developed for CIMR that uses empirically retrieved parameters of the relation between measured brightness temperature and modeled sea ice thickness to obtain sea ice thickness estimates.

In this thesis, I have created a new data set with more regions, more years from 2011 to 2020, and a longer period for the initial ice growth phase up to thick first year ice to analyze these parameters for consistency and regional differences, since the current parameters are estimated with only sparse data. Using SMOS L-band brightness temperatures and two simple models to simulate sea ice thickness growth, I investigate the brightness temperature evolution in the Arctic and Antarctic and separate different physical effects contributing to the L-band signal, where I particularly study ice thickness, snow depth and temperature. The analysis showed no regional difference for either parameter. However, a higher value of one parameter can be detected compared to previously retrieved parameters for the CIMR algorithm. This thesis demonstrates for the Arctic that the current CIMR parameters do not represent the relation between brightness temperature and sea ice thickness for my data set. Further investigation into the temporal evolution of the parameters shows that only a slight positive trend was found for one parameter. In addition, a relation between snow thickness and brightness temperature was found in Antarctica.

Contents

List of tables

List of figures

List of Abbreviations

TB	brightness temperature
SIT	sea ice thickness
SIC	sea ice concentration
ST	snow thickness
MIRAS	Microwave Imaging Radiometer using Aperture Synthesis
SMOS	Soil Moisture and Ocean Salinity
SMAP	Soil Moisture Active Passive
CIMR	Copernicus Imaging Microwave Radiometer
NASA	National Aeronautics and Space Administration
ESA	European Space Agency
RFI	Radio Frequency Interference
CFDD	Cumulative Freezing Degree Days
ATBD	Algorithm Theoretical Basis Document
NCEP	National Centers for Environmental Prediction

1 Introduction

Sea ice affects the Earth's weather and climate and is therefore an important climate parameter (IPCC, 2022). Observations and knowledge of sea ice are crucial for understanding and predicting climate change. In recent decades, the extent and volume of Arctic sea ice has changed dramatically and at an unprecedented rate. Arctic sea ice is melting, sea ice thickness and sea ice area are decreasing and a new minimum in Arctic sea ice extent is recorded almost every year. The rapid decline in the extent and thickness of the Arctic sea ice cover is one of the most visible signs of global climate change (IPCC, 2022).

Sea ice thickness (SIT) is one of the key parameters characterizing and influencing the Earth's climate and ocean-atmosphere heat exchange in the polar oceans (IPCC, 2022). It reflects a large fraction of incoming solar radiation back to space and thus has an tremendous impact on the high-latitude heat-budget. Even a thin layer of sea ice provides thermal insulation, inhibits evaporation, reduces ocean-atmosphere heat and gas exchange, and increases the albedo. In addition, sea ice also provides a solid surface for snow deposition, further reducing heat exchange and increasing albedo (IPCC, 2022). SIT is used not only for estimating the high-latitude heat-budget or sea-ice volume, but also for ship navigation, as well as to assimilate SIT data into regional ice prediction and global climate models (Gupta et al., 2019). SIT products are essential for ship operations and for understanding, modeling, and predicting sea ice, weather, and climate (Huntemann et al., 2014; Paţilea et al., 2019). Therefore, observations and the accurate representation of SIT and improved retrievals are important and necessary for various application fields.

The Arctic Ocean covers about 15.5 million square kilometers around the Earth's North Pole. In the past, most of the surface of the Arctic Ocean was covered with ice throughout the year. This has changed with global climate change. This core of perennial ice is surrounded by a rim of seasonal ice that freezes each winter and melts each summer. Consequently, Arctic sea ice extent peaks in March and troughs in September (Lindsey & Scott, 2022).

The sea ice extent in the Arctic Ocean, the total area of the Arctic with at least 15 % sea ice concentration, has been decreasing since continuous satellite measurements of sea ice extent began in 1978. The long record shows statistically significant negative trends in mean sea ice extent for each of the 12 calendar months (very high confidence), with the largest changes in summer and the smallest in winter (IPCC, 2022; Parkinson, 2022). The strongest trends for summer and winter occur in September (1979-2018; summer month with the lowest sea ice extent) with a negative trend of -83,000 km^2/yr per decade (-12.8 % ± 2.3 %) relative to the 1981-2010 average, and in March (1979-2019; winter month with the highest sea ice extent) with a negative trend of -41,000 km^2/yr per decade (-2.7 % ± 0.5 %) relative to the 1981-2010 average, respectively (Meredith et al., 2022).

Although the extent of sea ice at the winter maximum in March has declined more slowly than the extent at the summer minimum in September, the winter ice pack is very different from what it used to be. The fraction of thick multi-year sea ice in the Arctic that is at least 5 years old declined from 30 % to 2 % between 1979 and 2018, and over the same period the fraction of thin first-year sea ice increased from about 40 % to 60-70 % (very high confidence) (Meredith et al., 2022). In addition, the sea ice thickness across the central Arctic decreased by 65 % between 1975 and 2012, from 3.59 m to 1.25 m (Meredith et al., 2022). Overall, the Arctic sea ice is becoming younger and thinner due to volume loss (very high confidence) (IPCC, 2022), showing an undeniable trend towards more ice melting in summer and less new ice forming in winter, and a marked shortening of the sea ice season across much of the marginal ice zone (Parkinson, 2022).

The IPCC (2022) states that about half of the observed Arctic summer sea ice loss is due to increased atmospheric greenhouse gas concentrations (medium confidence). In addition, the shift to younger and thinner seasonal sea ice reinforces other processes that favor further reductions in sea ice extent. Not only is the first-year sea ice more fragile and vulnerable to summer melt through increased energy absorption and waves and storms (Arctic cyclones), and less likely to survive the summer than in the past, but feedbacks or other processes are also enhanced. For example, the sea ice albedo feedback, which is a key driver of sea ice loss and is intensified by the change from perennial to seasonal sea ice (Meredith et al., 2022). Increased air temperature reduces the sea ice cover and hence surface albedo, allowing more solar radiation energy to be absorbed by dark, low-albedo ocean or land surfaces with, causing additional warming and further sea ice reductions, further accelerating this feedback. This feedback loop is known as Arctic Amplification.

“Changes in Arctic sea ice have the potential to influence mid-latitude weather on timescales of weeks to months (low to medium confidence)” (IPCC, 2022) and contribute to sea level rise. The noticeable decrease and change in the extent, thickness and volume of Arctic sea ice raises the question of the magnitude and impact of SIT changes on climate and the environment. Accurate SIT data and improved current retrievals are needed, to better understand, model, and predict sea ice, weather, and climate.

SIT is measured on a large scale by satellites using a variety of techniques. Active instruments such as radar or laser altimeters can retrieve SIT with freeboard measurements and Archimedes’ law, but have large uncertainties for ice thicknesses less than 1 m (Kaleschke et al., 2012; Maaß et al., 2015). Furthermore, altimeters only provide thickness maps with a spatial resolution of about 25-100 km and monthly coverage (Tian-Kunze et al., 2014). Thermal infrared imagery, on the other hand, can detect SIT up to about 0.5 m from ice surface temperature measurement, but can only be used in cold, cloud free conditions, which is not very suitable in the Arctic (Kaleschke et al., 2012; Maaß et al., 2015). Only passive microwave radiometry can provide continuous, all-weather coverage of SIT at different spatial resolutions throughout the Arctic and Antarctic (Gupta et al., 2019). Observations of microwave emissions are not affected by the atmosphere, clouds or rain, because the wavelengths are much larger than the droplet size, and provide information on thin SIT up to about 1 m (Hosoda, 2010; Paţilea et al., 2019).

There are different satellites operating in the microwave frequency spectrum. For example, ESA's SMOS mission, launched in 2009, carries a passive microwave radiometer that operates at 1.4 GHz (L-band) and measures brightness temperatures. Another satellite for 1.4 GHz observations would be SMAP, launched by NASA in 2015. (Schmitt & Kaleschke, 2018) Microwave emissions from ice depend on certain microphysical properties, such as sea ice thickness, ice salinity, ice temperature, and snow grain size (Huntemann et al., 2014). Within one SMOS footprint, the brightness temperature depends mainly on the ice concentration, the molecular temperatures of the sea and the ice, and their emissivity (Tian-Kunze et al., 2014). Kaleschke et al. (2010; 2012) showed that microwave emissions at this low frequency are sensitive to ice thickness up to about 50 cm, and even greater to ice of less saline waters such as the Baltic Sea. Different methods, algorithms and approaches have been used to retrieve thicknesses of thin, young first-year ice in the winter freeze-up period from brightness temperature data. Two SIT retrieval algorithms are the one from Tian-Kunze et al. (2014), which is used in the official ESA SMOS SIT product, and the one from Huntemann et al. (2014), which is used at the University of Bremen for a thin SIT dataset.

A new satellite for the European Copernicus program's CIMR mission is expected to be launched in 2029. The microwave radiometer imager on board the CIMR satellite will measure global microwave emissions at various frequencies, including 1.4 GHz, and will operate at an incidence angle of 53° (G. Spreen, personal communication, October 5, 2022) (ESA, 2023). For this reason, a new SIT retrieval for CIMR L1b brightness temperatures has recently been developed by Marcus Huntemann and Gunnar Spreen based on the algorithm of Huntemann et al. (2014) and Paţilea et al. (2019). It is an empirical algorithm that is trained based on modeled ice thicknesses during the 2010 freeze-up period in the Kara and Barents Seas from a Cumulative Freezing Degree Days (CFDD) model and SMOS brightness temperatures at 53° incidence angle. Using a simple exponential analytical equation with three parameters, a least squares fit is made to the modeled SIT and the horizontal and vertical brightness temperature (TB) data to empirically determine the coefficients and to obtain a dependence of TB on ice thickness, which is then used for the retrieval.

The goal of this thesis is to evaluate the new retrieval algorithm developed by Huntemann and Spreen for the CIMR mission by analyzing the coefficients of the fit function used for consistency for the initial ice growth phase up to thick first year ice in the Arctic. Throughout this work, I compare the parameters of the fit function for the CIMR algorithm with newly obtained parameters using training data from different regions of the Arctic and a much longer time span. I am investigating whether the currently used training data for the algorithm from one freeze up period in almost one region is representative for the whole Arctic and whether more training data lead to different results in the coefficients for the retrieval. Using many years of L-band SMOS brightness temperature data, I will examine whether the current fit parameters of the CIMR retrieval are consistent with parameters calculated using training data from five different Arctic regions and ten years of observations. I will also analyze the possibility of regional differences or temporal evolution in the different parameters and the extent to which brightness temperature is sensitive to changes in ice thickness.

I will use SMOS observations data from 2011 to 2020 in five different regions in the Arctic and modeled SIT from the CFDD and another thermodynamic energy balance model. This will allow a comparison between the two models, and since the thermodynamic model simulates snowfall separately, it will allow to investigate the relation between snow thickness and the L-band signal. In addition, I analyze the sensitivity of the retrieval algorithm and extend the analysis to the Antarctic, although the ice growth in the Antarctic is different from the Arctic. I will investigate if the parameters show differences to the calculated CIMR values and do a sensitivity analysis as well.

The analysis with much more data can have a direct impact and hopefully improve the SIT retrievals of CIMR in the future. It is important, to determine SIT more precisely and to make retrieval algorithms as accurate as possible, because uncertainties in SIT and insufficient knowledge about them lead to inaccurate results in further processing and modeling. Because the use of SIT is so diverse, the correct and accurate representation of SIT is therefore of immense importance for science and other purposes.

Section 2.1 provides information on the observation of SIT and its history. The SMOS and CIMR missions are described in Sections 2.2 and 2.3, respectively. A brief description of the brightness temperature and the L-band brightness temperature is given in Section 2.4. The retrieval methods, in particular the retrieval method of Huntemann et al. (2014) and the new CIMR algorithm, are presented in Section 2.5. The data and models used in this thesis are described in Chapter 3, the results and methods are presented in Chapter 4 and are summarized in Chapter 5. A discussion and conclusion follow in Chapter 6.

2 Background

2.1 Observation of sea ice thickness

There are several ways of measurements that can be used to obtain information about SIT. These can be divided into invasive (in situ on-ice measurements) and non-invasive (remote sensing) methods (Gupta et al., 2019). There are some campaigns to study sea ice and especially thicker ice with invasive measurements, such as the MOSAiC expedition. However, especially the in situ observation of thin sea ice has its difficulties. Because it is not possible to stand or walk on it, there are basically no on-ice observations of thin sea ice. This is why the use of remote sensing methods is so important. Non-invasive methods include for example helicopter-based electromagnetic (EM) induction, upward-looking sonar (ULS), ICESat laser altimeter, Cryosat-2 radar altimeter ice freeboard measurements, and passive microwave radiometry (Gupta et al., 2019).

Three main methods have been used to retrieve SIT from satellites. (1) It can be derived from sea ice freeboard measurements using altimeters and Archimedes' law. However, this method results in large relative errors for thin sea ice (Kaleschke et al., 2012; Maaß et al., 2015). (2) Another method for assessing the thickness of thin sea ice up to about 0.5 m would be to estimate it from the temperature of the ice surface using thermal infrared imagery. The major drawback of this retrieval is the requirement for cold clear sky conditions and the interference of fog and thin clouds (Kaleschke et al., 2012; Maaß et al., 2015). This would result in large temporal gaps in ice thickness observations.

(3) A much better method for determining sea ice thickness is microwave emission measured by satellites. Because of the long wavelengths in the microwave spectrum, scattering and absorption by aerosols is usually negligible, and because the wavelengths are much larger than the droplet sizes, the observations are not affected by clouds and rain (Hosoda, 2010; Thomas Wagner, 18.12.18). It can be said that the atmosphere is nearly transparent at these low frequencies (Paţilea et al., 2019). The major advantage of passive microwave radiometry is that this method does not have problems with spatial coverage and continuous measurements, unlike altimeters, which are swath-limited, or helicopter-based electromagnetic induction and ULS, which provide only sparse spatial coverage. Passive microwave radiometry provides continuous, all-weather coverage of SIT at various spatial resolutions throughout the Arctic and Antarctic (Gupta et al., 2019).

With this method, the Earth's surface can be measured during the day and night and in almost all-weather conditions.

Satellites observations of sea ice have a long history. For more than 40 years, the sea ice concentration and coverage have been observed by several satellite-based passive microwave radiometers (Yang et al., 2014). The ongoing satellites are the Special Sensor Microwave Imager (SSM/I) (1987–present) and the Advanced Microwave Scanning Radiometer 2 (AMSR2)

(2012–present) (Huntemann et al., 2014). Satellite observations of sea ice thickness began with radar altimeters on the European Remote Sensing Satellites (ERS-1 and ERS-2) launched in the 1990s (Tian-Kunze et al., 2014), and thermal imagery from the Advanced Very High Resolution Radiometer (AVHRR) launched in 1979 (Tian-Kunze et al., 2014). The ICESat laser altimeter, which was operational from 2003 to 2009, the ICESat-2 laser altimeter, which has been operational since 2018, and the CryoSat-2 radar altimeter, which has been operational since 2011, follow these early radar altimeter observations (Tian-Kunze et al., 2014). One problem with radar and laser altimeters is that they have large uncertainties for ice thicknesses less than 1 m, making them suitable for thick ice detection but not for thin ice (Tian-Kunze et al., 2014). In addition, altimeter ice thickness maps typically have a temporal resolution of one month and a spatial resolution of about 25-100 km, making these ice thickness data unsuitable for forecasting systems that require daily updates and high spatial resolution (Tian-Kunze et al., 2014; Yang et al., 2014).

To overcome these limitations in terms of temporal and spatial resolution, attempts have been made to estimate ice thickness from passive microwave measurements on the 19-90 GHz channels, for example using passive microwave radiometer data from the Special Sensor Microwave Imager (SSM/I) (37 and 85.5 GHz channels) and the Advanced Microwave Scanning Radiometer-Earth Observing System (AMSR-E) (36.5 and 89 GHz channels) sensors for example (Tian-Kunze et al., 2014). Because of the correlation between ice thickness and ice surface salinity, these data have been used to estimate ice thickness (Maaß et al., 2015). However, this microwave method, based on correlations between surface properties and thickness, is only valid for ice thicknesses less than 10–20 cm (Kaleschke et al., 2012). Although the spatial resolution of radiometer-based maps of thin ice thickness (6.25 to 25 km) is much coarser than that of thermal imagery, it is still possible to obtain daily coverage of the Arctic and Antarctic (Tian-Kunze et al., 2014). One problem with this retrieval is that quantification of thin ice thickness with 37 and 90 GHz data is not possible when the ice is covered by snow or has a high area fraction of frost flowers (Maaß et al., 2015).

In 2009, the European Space Agency (ESA) launched a satellite for the Soil Moisture and Ocean Salinity (SMOS) mission to provide global observations of soil moisture over land and salinity over oceans. The passive microwave radiometer operates in the 1.4 GHz (L-band) microwave range to acquire brightness temperature images over a range of incidence angles from 0 to about 70° (Schmitt & Kaleschke, 2018). These 1.4 GHz TBs have also been used to try to obtain information on SIT. Since the atmosphere has a negligible effect on the TB at this low frequency, snow is almost transparent at L-band (Huntemann et al., 2014), and other studies such as Kaleschke et al. (2010; 2012) have shown sensitivity to ice thickness up to 50 cm (Paţilea et al., 2019), the 1.4 GHz TB data can be used to retrieve SIT. Some retrieval methods and algorithms for L-band SIT retrieval are further described in Section 2.5. The SMOS mission provides a new complementary satellite-based dataset with daily coverage and a long continuous timespan for estimating sea ice thickness (Maaß et al., 2015). A detailed overview of the SMOS mission and the satellite data, which is used in this study, is given in Section 2.2 and 3.1, respectively.

Further opportunities for SIT measurements include the Soil Moisture Active Passive (SMAP) satellite launched by NASA in January 2015. It also detects microwave TB at 1.4 GHz and makes observations of soil moisture and freeze/thaw conditions in the surface soil everywhere on Earth. The observations provide greatly improved estimates of the transfer of water, energy, and carbon between the land and the atmosphere and their maintenance of our climate and environment (Dara Entekhabi et al., 2014). The SMAP satellite, unlike SMOS, has to instruments on board, a radar (active) and an L-band (1.4 GHz) microwave radiometer (passive). They share a rotating 6 m real aperture antenna reflector and together they make global measurements of land surface soil moisture and freeze/thaw state every 2-3 days (Balsamo et al., 2018; Dara Entekhabi et al., 2014). Although the radar, used to acquire high-resolution (1 to 3 km) data for soil moisture sensing and freeze/thaw mapping, failed after 3 months (Paţilea et al., 2019), the radiometer is still operating and mapping soil moisture at 36 km spatial resolution. After the failure of the radar, the radiometer data were used to produce the freeze/thaw map at a resolution of 36 km (Dara Entekhabi et al., 2014).

The SMAP observations, whose primary mission is on soil moisture retrieval and freeze/thaw detection, have also been used for ocean salinity and wind retrieval (Balsamo et al., 2018), and can also be used for SIT retrieval. However, in contrast to SMOS, the SMAP mission measures brightness temperature data at a fixed incidence angle of 40° (Paţilea et al., 2019), which means that data products need to be converted between the two sensors. However, this opens up new possibilities for SIT retrieval. With adapted algorithms and new approaches, the TB from SMAP can be used to obtain a combined SMOS-SMAP thin SIT product and a better spatial and temporal coverage (Paţilea et al., 2019).

And the latest possibility for SIT measurements in the near future may be another satellite, which is expected to be deployed by 2029 for the Copernicus Imaging Microwave Radiometer (CIMR) mission of the European Copernicus program. The CIMR mission will observe global multi-frequency microwave radiometric images of TB at 53° incidence angle, focusing on high latitude regions (ESA, 2023). It will provide observations of sea surface temperature (SST), sea ice concentration (SIC) and sea surface salinity (SSS). And the data can be used to observe other sea-ice parameters such as sea ice thickness and drift (ESA, 2020). This will allow European researchers to better understand the changing conditions in the Arctic and how to support the most affected people in these regions (ESA, 2020). The CIMR mission is currently in the preparatory phase and the CIMR satellite will carry a microwave radiometer imager operating in five spectral bands at frequencies of 1.4, 6.9, 10.65, 18.7, and 36.5 GHz. It is designed for a nominal lifetime of 7 years and, with its three satellites, will enable subdaily observations and a continuous day and night monitoring of the Arctic and Antarctic (ESA, 2020). For more information on the CIMR mission and the data it will produce, see Section 2.3.

The CIMR satellite data will also be used to derive SIT estimates. Marcus Huntemann and Gunnar Spreen are developing an algorithm based on Huntemann et al. (2014) and Paţilea et al. (2019) for a SIT retrieval with CIMR L1b brightness temperatures. This algorithm is explained in Section 2.5 and in the Algorithm Theoretical Basis Document (ATBD) (Huntemann & Spreen, 2022).

There are many ways to measure SIT. Some methods have more advantages and are more suitable than others, but with continuous data over longer periods of time, that can be worked with because of satellite measurements, better and more accurate algorithms can be developed to detect changes and produce more accurate maps and SIT products with higher spatial or temporal resolution. Especially with new products that combine coarser resolution remote sensing capabilities (e.g., SMOS/SMAP) with high resolution imagers, the SIT product may be even less limited in spatial and temporal resolution. These combined products hold great promise for supporting and advancing the development of the next generation of weather and climate models, which will approach kilometer-scale resolution at the surface (Balsamo et al., 2018).

With these data, it will be possible to produce better climate scenarios and models, to make more reliable weather predictions and forecasts, and to integrate these data into existing climate and weather models and develop new ones.

2.2 SMOS mission

ESA's (European Space Agency) Soil Moisture and Ocean Salinity (SMOS) mission is one of the Earth Explorer Missions of the Living Planet Earth Observation Program. The program is investigating global environmental change and individual aspects of the Earth's environment, climate, and composition. The goal of the SMOS mission is to improve our understanding of the water cycle and our ability to forecast weather by providing global observations and information on soil moisture and ocean salinity.

Launched in November 2009, SMOS carries a single instrument called the Microwave Imaging Radiometer using Aperture Synthesis (MIRAS) which measures the Earth's natural emission at a relatively low microwave frequency of 1.4 GHz (Balsamo et al., 2018). With its 69 receivers, it measures the phase difference of incidence radiation from an area at different angles, providing a much more detailed picture than a single receiver (ESA, 2012). (see Section 3.1 for details) SMOS is designed to retrieve soil moisture and sea surface salinity and provides brightness temperature data in the L-band (1.4 GHz). The amount of microwave radiation emitted is affected by moisture and salinity, which reduce the emissivity of soil and seawater, respectively. Because of the large dielectric contrast between dry soil and water, the soil emissivity at a specific microwave frequency depends on the moisture content. Especially in L-band, the sensitivity to soil moisture is very high, while the sensitivity to atmospheric interference and surface roughness is minimal (ESA, 2012). Because of this correlation between moisture content and surface emissivity, soil moisture can be inferred from brightness temperature observations (Paţilea et al., 2019). Sea surface salinity can be inferred from brightness temperature because the ocean surface emissivity is a function of the dielectric constant and the state of the surface roughness (ESA, 2012). The dielectric constant for seawater is determined by electrical conductivity and microwave frequency. Since the measured brightness temperatures are related to the salinity of the sea through the dielectric constant of the water in the first few centimeters, the sea surface salinity can be retrieved (Paţilea et al., 2019).

The obtained SMOS brightness temperature data have not only been used to determine soil moisture and sea surface salinity, but also numerous studies have been conducted in various Earth applications to investigate the relationships with soil moisture, sea surface salinity, sea ice concentration, snow thickness and also thin sea ice thickness (Gupta et al., 2019).

Simultaneous airborne measurements of L-band brightness temperature and ice thickness from electromagnetic induction measurements during the 2007 Pol-ICE campaign in the Baltic Sea demonstrated the potential for deriving sea ice thickness from L-band radiometry (Maaß et al., 2015). Further modeling and observations have shown that radiation at this frequency is sensitive to ice thickness up to 50 cm, and that the penetration depth into sea ice is about 50 cm, and even greater into ice of less saline waters such as the Baltic Sea (Huntemann et al., 2014; Paţilea et al., 2019). The small influence of the atmosphere, because both absorption and scattering are small and the atmosphere is therefore nearly transparent, on the emitted microwave radiation in the low frequency L-band and the correlation of ice thickness with this radiation make SMOS a candidate for thickness measurements of thin sea ice (Paţilea et al., 2019).

The SMOS brightness temperature data have been used since 2009 for the thickness retrieval of thin Arctic sea ice up to about 50 cm, and Kaleschke et al. (2010) expected that this retrieval would also be suitable for thicker low-salinity ice (Maaß et al., 2015). The obtained estimates of thin sea ice thickness have already been successfully integrated into forecast models to constrain the ice analysis, leading to more accurate initial conditions and thus more accurate forecasts (Richter et al., 2018). Since the SMOS-derived ice thickness has less uncertainty than ICESat and CryoSat-2 measurements for thin sea ice (< 50 cm), but exponentially increasing uncertainty for thick sea ice (> 50 cm), the sea ice thickness derived from SMOS can complement the overall Arctic-wide SIT product (Tian-Kunze et al., 2014). This opens up new opportunities and new fields of study for a better understanding of sea ice evolution and its predictability.

2.3 CIMR mission

The Copernicus Imaging Microwave Radiometer (CIMR) is a high-priority satellite mission in the Copernicus program (ESA, 2023). The European Copernicus Program is a system for monitoring the Earth in support of European policies and is the world's largest provider of Earth observation data (ESA, 2023). It aims to continuously record the current state of the Earth and to provide data processing services derived from satellite and in-situ (non-space) observations in order to provide users such as public authorities, companies, institutions, environmental agencies and citizens with reliable and up-to-date information through a set of Copernicus operational services related to environmental and security issues (ESA, 2023). The information services cover Atmosphere, Marine and Land Monitoring; Climate Change; Emergency Management and Security and are provided free and open to users (ESA, 2023).

The Copernicus program is coordinated and managed by the EU, represented by the European Commission. It is conducted in partnership with the Member States, the European Organization for the Exploitation of Meteorological Satellites (EUMETSAT), the European Space Agency (ESA), which develops, builds, launches and operates the associated satellites together with its partner EUMETSAT, the European Centre for Medium-Range Weather Forecasts (ECMWF), EU agencies and Mercator Océan.

The CIMR mission is considering the inclusion of global multi-frequency imaging microwave radiometry with a focus on high latitude regions in support of the European Union's (EU) Integrated Arctic Policy (ESA, 2023). More recently, the European Commission (EC) has set new objectives related to improved spatial and temporal coverage of sea ice and the Arctic environment to support Arctic user communities (ESA, 2020). The CIMR mission is in the preparation phase and is expected to be launched in 2029. CIMR will provide observations of sea surface temperature (SST), sea ice concentration (SIC) and sea surface salinity (SSS) using a microwave radiometer. In addition, the satellite will observe other sea-ice parameters such as sea ice thickness and drift (ESA, 2023). These three main parameters will allow European researchers to better understand the changing conditions in the Arctic and how to support the most affected people in these regions (ESA, 2020).

The CIMR satellites will carry wide-swath, conically-scanning, multi-frequency microwave radiometer imagers with a complex antenna structure that can be deployed in space (ESA, 2020). The instrument will continuously rotate about a local vertical axis to maintain a high swath width throughout the orbit (ESA, 2020). The satellites are expected to operate in a quasi-polar, nearly circular, sun-synchronous orbit at an altitude of approximately 817 km (ESA, 2020). CIMR will have a repetition rate of 1.5 days and is designed for a nominal lifetime of 7 years (ESA, 2020). Based on current expectations, the number of satellites in the mission will be limited to three, allowing for a continuous day and night monitoring of the Arctic and Antarctic and providing subdaily observations of the Arctic and Antarctic (ESA, 2020).

The microwave radiometer imager will operate at 53° incidence angle in L-band (1.4 GHz) and at 55° incidence angle in four spectral bands at frequencies of 6.9, 10.65, 18.7, and 36.5 GHz, providing brightness temperature data (G. Spreen, personal communication, October 5, 2022). The three target parameters SIC, SST and SSS will be imaged at different resolutions (ESA, 2020). The SIC will be recorded with a spatial resolution of 5 km, an uncertainty of < 5 % and a subdaily temporal sampling period. The SST will be recorded more coarsely with a spatial resolution of 15 km, an uncertainty of < 0.3 K, and also with a subdaily temporal sampling. The SSS will again be recorded with a finer resolution of 5 km, an uncertainty of < 0.3 pss (Practical Salinity Scale), but will be sampled only once a month (ESA, 2020).

The continuity of measurements of thin sea ice (< 0.5 m depth) by L-band microwave radiometry with daily coverage North of 55° as well as in Antarctica is requested in several expert group user requirement documents for the CIMR mission (ESA, 2023).The reason for this requirement is that sea ice modelers and operational ice services consistently place the highest priority on improved measurements of sea ice thickness distribution (ESA, 2023). And in the absence of a high spatial resolution thin sea ice thickness product in the Arctic Ocean, complete daily collection and near real-time availability of thin sea ice thickness data would be helpful for operational applications such as navigation (ESA, 2023). The Mission Requirements Document (ESA, 2023) also states that since the assimilation of thin (< 0.5 m) sea ice thickness data derived from L-band (1.4 GHz) satellite missions into dynamic sea ice models leads to more accurate forecasts, it is important to ensure the continuity of L-band measurements in an operational context.

Furthermore, the ability to derive thin SIT complements the proposed topography SARIn altimeter mission measurements of sea ice freeboard, as an altimeter is unable to provide meaningful ice thickness measurements much below 1 m (ESA, 2023). In addition, the CIMR mission will provide supplementary information on snow loading (“snow depth on sea ice”) to support the topography mission measurement of sea ice thickness derived from sea ice freeboard estimates (ESA, 2023).

2.4 Brightness temperature

Brightness temperature (TB) characterizes radiation. It is a measure of the radiance of microwave radiation traveling upward from the top of the atmosphere to the satellite, expressed in units of the temperature of an equivalent black body.

The amount of electromagnetic radiation emitted by a black body in thermal equilibrium at a given temperature is described by the Planck's law:

$$I = \frac{2hv^3}{c^2}\frac{1}{\exp(\frac{hv}{kT}) - 1} \tag{2.1}$$

Where I (intensity or brightness) is the amount of energy emitted, h is the Planck's constant, v is the frequency, c is the speed of light, T is the temperature of the black body, and k is the Boltzmann constant.

In this work, the SMOS brightness temperatures at 1.4 GHz are used, and since the received signal is in the microwave spectrum, i.e. low frequency, therefore $hv \ll kT$, we can use the Rayleigh-Jeans law:

$$I = \frac{2v^2kT}{c^2} \tag{2.2}$$

The Rayleigh-Jeans law is an approximation for the spectral radiance of electromagnetic radiation at low frequencies. Because of the relation, the observed signal (spectral radiance) is proportional to T of measured object at a given frequency and has a square dependence on v.

For a grey body, the spectral radiance is a fraction of the black body radiance, determined by the emissivity ε, so the brightness temperature can simply be written as:

$$TB(p,f) = \varepsilon(p,f) * T_{Blackbody} \tag{2.3}$$

The emissivity is still dependent on the polarization p and the frequency f of the radiation (Huntemann, 2015). Here the assumption of an infinite half-space of the material is made, which is a typical assumption for microwave remote sensing of sea ice. That means that T is independent of depth (Huntemann, 2015). For a black body (ε = 1), the brightness temperature is equal to the temperature of the black body. For grey bodies with emissivities ε between 0 and 1, the observed brightness temperature is less than the true temperature and a reflected component comes into play.

2.4.1 Brightness temperature at L-band

Certain microphysical properties, such as sea ice thickness, ice salinity, ice temperature, and snow grain size, determine the sensitivity of microwave emission from sea ice (Huntemann et al., 2014). The L-band brightness temperature measured at 1.4 GHz in one SMOS footprint depends mainly on the ice concentration, the molecular temperatures of the sea and the ice, and their emissivity (Tian-Kunze et al., 2014). And the emissivity of sea ice in turn depends on certain factors such as salinity and the microphysical structure of the sea ice (Tian-Kunze et al., 2014). Inhomogeneities in the sea ice such as brine pockets and air bubbles alter the microphysical structure of sea ice, but since they are much smaller than the SMOS wavelength of 21 cm, we can consider sea ice as a homogeneous medium and ignore volume scattering (Tian-Kunze et al., 2014).

There are other uncertainties associated with the SIT retrieval at L-band. Wang et al. (2010) stated that the uncertainty in snow thickness is typically one of the main factors determining the uncertainty of the retrieved ice thickness. Although snow is almost transparent at L-band, the indirect influence of thermal insulation by the snow layer has a strong impact on the retrieval (Tian-Kunze et al., 2014). Huntemann et al. (2014) also suggest that snow cover and temperature have the strongest influence on the retrieval. The thermal insulation leads to higher ice temperatures and thus to a higher polarization difference (the difference between the intensities observed at vertical and horizontal polarization), increased brine volume, a higher permittivity and thinner thickness retrievals (Huntemann et al., 2014). In addition, there are other factors that play an important role in observing and determining sea ice thickness. For example, the inhomogeneous, anisotropic, and heterogeneous nature of the sea ice surface and the invisible sea ice bottom introduce uncertainties in SIT estimates, which in turn lead to uncertainties in sea ice volume estimates due to error propagation (Gupta et al., 2019). Other problems with current SIT retrievals include sea ice drift, breakup of leads by currents and winds, snow and ice roughness, ice thickness distribution, ice salinity and temperature, and differentiation between thin SIT and low SIC (Gupta et al., 2019; Paţilea et al., 2019).

SMOS provides horizontal and vertical polarized brightness temperatures (TB_h and TB_v, respectively) at incidence angles between 0° and 65°. Figure 2.1 shows the basic brightness temperature situation over sea ice and open water. At nadir, the TB of open water is about 100 K. For horizontal polarization, the TB decreases with incidence angle down to 60 K at 65°, while for vertical polarization the TB increases to about 180 K at 65° (Huntemann et al., 2014). The TB for sea ice is higher for all incidence angles and is about 230 K at nadir. For horizontal polarization, the TB decreases to 215 K at 65° and for vertical polarization it increases to 260 K at 65° (Huntemann et al., 2014). The high TB contrast between ice and water of about 100 K and the high penetration depth at L-band allow to evaluate the potential of SIT detection with SMOS (Gupta et al., 2019). For observations of up to 40° incidence angle, Kaleschke et al. (2010; 2012) were the first to show that the intensity (the average of horizontally and vertically polarized brightness temperatures) can be used to provide information on sea ice thickness (Huntemann et al., 2014).

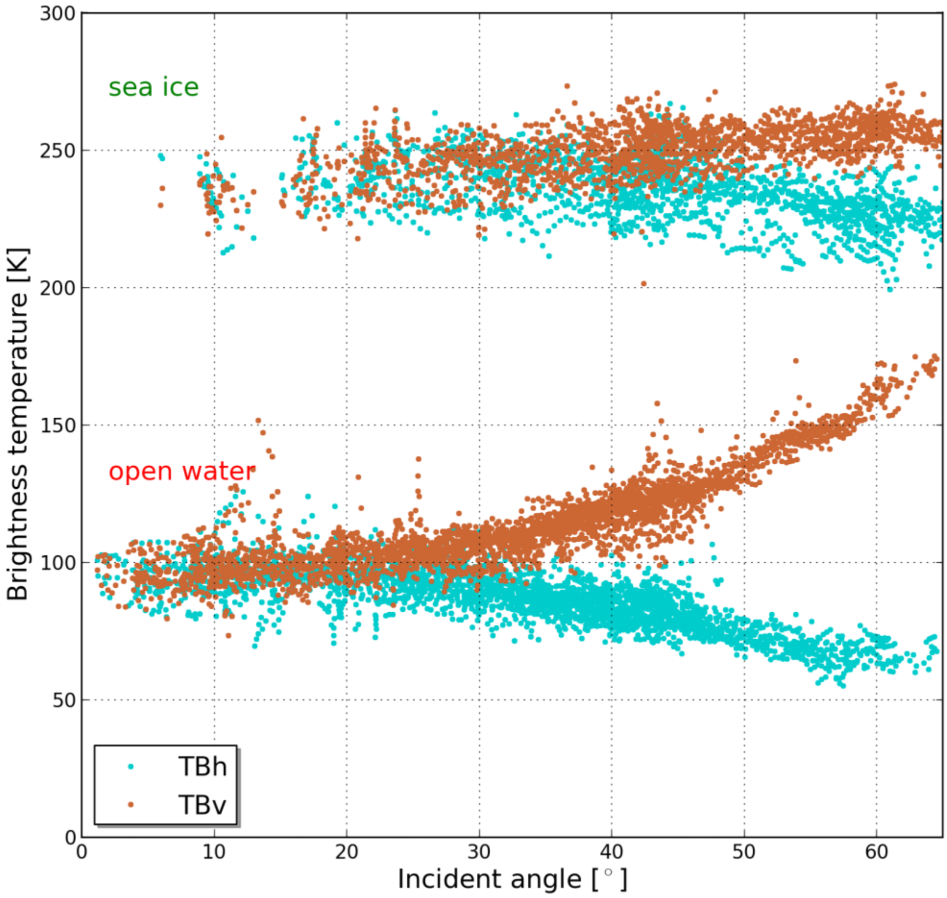

Figure 2.1: TB dependence on the incidence angle
TB dependence on the incidence angle for horizontal (blue) and vertical (brown) polarization for sea ice and open water. Testing large area of brightness temperatures throughout the whole Arctic area from 20 April 2012.
Source: Huntemann et al. (2014, p. 440)

However, there are limitations to the L-band SIT retrievals. Because the footprint has a resolution of about 50 km, there can be water and ice in one footprint. This means that regions of thin ice at the edges will not be retrieved correctly. Also, the occurrence of liquid water content at the snow-air and snow-ice interface in one footprint leads to a dramatic change in the TB (Gupta et al., 2019). For this reason, the retrieval is limited to the freezing season and is not applicable during the melting season. During the melt season, the thickness of sea ice is highly variable, and the sea ice cover is too inhomogeneous. With the mixture of wet sea ice, melt ponds, and open water within one SMOS footprint, the retrieval would not yield meaningful results (Huntemann et al., 2014). Even during the freezing season, heavy rainfall or melting can produce misleading results. The SIT retrieval with TB is therefore limited to the cold and dry season from October to April in the Arctic and from March to September in the Antarctic (Gupta et al., 2019; Huntemann et al., 2014).

2.5 Retrieval Methods

After the launch of SMOS, there are several SIT retrieval methods that use SMOS TBs from L-band and relate the emitted radiation to ice thickness. As mentioned above, in this section the method by Huntemann et al. (2014) and the new CIMR algorithm are discussed in more detail and other methods are briefly described. Currently used methods are those of Tian-Kunze et al. (2014) and Huntemann et al. (2014). Tian-Kunze et al. (2014) use the TB intensity averaged over incidence angles between 0° and 40°, and Huntemann et al. (2014) use TB intensity and polarization difference averaged over incidence angles between 40° and 50° to derive SIT. The algorithm of Tian-Kunze et al. (2014) is used in the official ESA SMOS SIT product and provides SIT values similar to the empirical method of Huntemann et al. (2014), although it extends the range of retrievable SIT values up to 1 m for growing sea ice under freeze-up conditions (Huntemann & Spreen, 2022). The empirical method from Huntemann et al. (2014) and SMOS TBs are used at the University of Bremen to release a thin SIT dataset.

The first demonstration study to derive SIT from SMOS L-band TBs was performed by Kaleschke et al. (2012). They derived thin SIT up to 50 cm for the Arctic freeze-up period using a semi-empirical algorithm with constant tie-points based on Level 1C brightness temperatures (Kaleschke et al., 2012; Tian-Kunze et al., 2014). They used averaged TB intensity over the incidence angle of up to < 40° and assumed a spatially homogeneous ocean, that is either ice free or 100 % covered by sea ice. Another strong simplification was made with constant retrieval parameters, which were derived from a sea ice radiation model for a representative temperature and salinity of sea ice in the Arctic (Tian-Kunze et al., 2014). They represent average freeze-up conditions in the Arctic. With all these assumptions made, Kaleschke et al. (2012) demonstrated the SMOS sea ice thickness retrieval method as proposed by Kaleschke et al. (2010) and found that “the time series provides clear evidence for a strong correlation between SMOS brightness temperature and sea ice thickness”.

The method used in the official ESA SMOS SIT product is that of Tian-Kunze et al. (2014). They extended the previously described method by considering varying ice temperature and salinity profiles within the ice column, which overcomes the major drawback of the constant temperature and salinity parameters of the algorithm by Kaleschke et al. (2012) (Gupta et al., 2019). The varying ice temperatures and salinities are estimated from surface air temperatures of atmospheric reanalysis data and a model based SSS climatology (Tian-Kunze et al., 2014). This more recent retrieval algorithm is based on a thermodynamic sea ice model and a three-layer radiative transfer model and allows SIT estimates of greater thicknesses up to ~ 1.5 m for cold conditions and less saline ice (Gupta et al., 2019). Due to dynamic-thermodynamic growth and deformation processes within the spatial resolution of SMOS, natural sea ice exhibits a statistical thickness distribution due to the mixture of thin and thick ice (Tian-Kunze et al., 2014). They statistically corrected the underestimation of ice thickness by implementing a lognormal function that approximates the ice thickness distribution function within the SMOS spatial resolution. The correction factor depends on the ice temperature and salinity. Tian-Kunze et al. (2014) found that the calculated ice thickness was in much better agreement with the validation data and had a more realistic Arctic-wide ice thickness distribution than the algorithm used in the previous study. A major drawback of this algorithm is that it is unable to distinguish areas of low SIC from areas of thin SIT, as both have similar TB (Gupta et al., 2019).

The second common SIT retrieval algorithm for SMOS is an empirical retrieval algorithm developed by Huntemann et al. (2014), which can detect thin SIT up to 50 cm during the freeze-up season. This method is also the basis for the new CIMR retrieval algorithm. The method uses brightness temperatures at higher incidence angles between 40° and 50°, which, in contrast to Tian-Kunze et al. (2014) for example, allows using not only the intensity, but also the polarization difference. Huntemann et al. (2014) found a high correlation to intensity and an anticorrelation to the polarization difference between SMOS brightness temperatures and thermodynamic ice growth data at these high incidence angles and used the intensity and polarization differences to fit an analytical equation to the dependency of TB and modeled ice thickness.

The training data used to fit the analytical equation are the L-band SMOS TBs averaged over 40°-50° and modeled ice thicknesses during the 2010 freeze-up period in the Kara and Barents Seas from the Cumulative Freezing Degree Day (CFDD) model (see 3.3 for details) with reanalysis data from the National Centers for Environmental Prediction (NCEP). For this purpose, 10 areas in the Kara and Barents Seas are used in their growing phase from October 1 to December 26, 2010. This area was chosen because the influence of sea ice drift from one day to the next can be neglected due to the small average sea ice drift of 8 km per day according to the low resolution ice drift product of the Ocean and Sea Ice Satellite Application Facility (OSI-SAF), which is about a half of the size of the 15 km grid cell used here, and because this area has a high sea ice concentration after the freeze-up according to AMSRE and SSM/I sea ice concentrations as retrieved by the ASI algorithm (Huntemann et al., 2014; Spreen et al., 2008).

Huntemann et al. (2014) analyzed the training data for consistency with SIT from the HIGHTSI and TOPAZ models, both of which contain the SIT directly, and found a high correlation of the SMOS TB_h and TB_v with the SIT from the models up to about 30-40 cm thickness. For further fitting of the equation, only CFDD derived SIT that show monotonic freeze-up periods, which occur in only 3 regions, are used. They also include observations with an initial increase in sea ice concentration from 0 to 100 % in the training data set, while excluding later decreases in SIC, possibly ice breakups, which was not done in previous SIT retrievals, in order not to neglect information from very thin sea ice, as current passive microwave algorithms yield ice concentrations below 100 % in the case of a thin ice cover. The SIT retrieval is cut off at 50 cm because the sensitivity of the retrieved SIT to both intensity and polarization difference increases strongly with SIT.

Equations (2.4) and (2.5) are fitted between the intensity I and the polarization difference Q and the SIT obtained from the CFDD model for the three selected regions.

$$I_{abc}(x) = B - (B - A) * \exp\left(-\frac{x}{C}\right) \quad (2.4)$$

$$Q_{abcd}(x) = (B - A) * \exp\left(-\left(\frac{x}{C}\right)^D\right) + A \quad (2.5)$$

A, B, C and D represent the parameters of the curves and x is the SIT. The parameters that best fit the training data are shown in Table 2.1. To obtain the SIT, the minimum Euclidean distance to the retrieval curve, which is the result of using the two fitted functions from Equations (2.4) and (2.5) in the I-Q-space, is used for each pair of Q and I.

Table 2.1: Fit parameters from Huntemann et al. (2014)
Parameters for best fit of the used training data in Huntemann et al. (2014) for Equations (2.4) and (2.5).

parameter	A [K]	B [K]	C [cm]	D
I_{abc}	100.2	234.1	12.7	-
Q_{abcd}	19.4	44.8	24.1	2.1

Although the SIT retrieval with this method shows a strong correlation with ice thickness data from airborne measurements and reasonable ice thickness patterns for the Arctic freeze-up period, comparison with data based on MODIS and EM bird measurements confirms that the retrieval gets worse for thicker ice, as the retrieval error is about 30 % of the retrieved SIT (3 cm for SIT below 10 cm, increasing to 16 cm for SIT between 40 and 50 cm) (Huntemann et al., 2014). The overall average error is 10 cm.

Huntemann et al. (2014) noted that temperature and snow cover may have the strongest influence on the retrieval, and that the accuracy could be improved by restricting the retrieval to near 100 % sea ice cover, since this approach, like the method of Tian-Kunze et al. (2014), also derives SIT in areas with SIC much less than 100 % (Gupta et al., 2019).

The newly modified SIT retrieval algorithm for CIMR, which is the subject of this paper, is presented by Gunnar Spreen and Marcus Huntemann. The Algorithm Theoretical Basis Document (ATBD) was developed as part of the CIMR DEVALGO study, which is a project to develop Level-2 algorithms for ESA's CIMR satellite (Huntemann & Spreen, 2022).

The new SIT retrieval algorithm for CIMR is based on the work of Huntemann et al. (2014) and Paţilea et al. (2019) and is modified in some aspects compared to the algorithm of Huntemann et al. (2014). The CIMR retrieval algorithm uses the method of Huntemann et al. (2014) instead of that of Tian-Kunze et al. (2014), which is used for the ESA SMOS SIT product, because the algorithm of Huntemann et al. (2014) uses TBs at incidence angles closer to the 53° incidence angle of CIMR, making it much more suitable for an adaptation to CIMR than that of Tian-

Kunze et al. (2014), which uses TBs close to nadir (0-40°) and thus does not consider polarization information (Huntemann & Spreen, 2022).

The CIMR algorithm is an empirical algorithm that, like Huntemann et al. (2014), is based on modeled ice thicknesses during the freeze-up period in the Kara and Barents Seas. But now it works with L-band TBs in horizontal and vertical polarization directly provided by the instrument at 53° incidence angle without any transformation, including their uncertainties, instead of TB intensity and polarization difference in the 40-50° incidence angle range as in Huntemann et al. (2014). The new algorithm also removes the forced upper limit of 50 cm of retrievable ice thickness, but it is now very loosely constrained by a background ice thickness. Although higher ice thicknesses do come with higher uncertainties, this may provide new opportunities for analysis and comparison. To evaluate the retrieval algorithm, SMOS brightness temperatures are compared with the ESA CCI Round robin data package and the ESA SMOS product (Huntemann & Spreen, 2022).

With this algorithm, CIMR L1b brightness temperatures will be processed into a L2b SIT product (i.e., swath-based sea ice thickness values in original footprint coordinates of the L1b data product), which will be provided in NetCDF format and includes the following variables: sea ice thickness, sea ice thickness standard error and sea ice thickness quality flag.

For the SIT retrieval algorithm, which uses the fitted parameters from individual fits of ice thickness to TBs and a minimization scheme including uncertainties using the error covariance matrix of TB_h and TB_v at 1.4 GHz, training data from Huntemann et al. (2014) are used to fit an analytical equation to the dependence of TB on ice thickness. The training data used for the fit are modeled ice thicknesses during the 2010 freeze-up period in the Kara and Barents Seas from a CFDD model and SMOS TBs at 53°, instead of averaged over 40°-50° as in Huntemann et al. (2014) or at 40° as in Paţilea et al. (2019). In contrast to Huntemann et al. (2014), all 10 regions are used to obtain the fit parameters, instead of only regions 3, 6 and 7; and points of open water with 0 cm SIT are now included, instead of being removed because they cause instability in the fitting procedure for the polarization difference Q (Huntemann & Spreen, 2022). The fit function used is the Equation (2.4), which is the same as that used in Huntemann et al. (2014). With A being the brightness temperature of open water close to sea ice under freezing conditions, B being the brightness temperature of thick sea ice, and C being a curvature parameter connecting the two TBs. The index indicates the polarization, either h or v. With this fit function, a least squares fit is made to the SIT and the horizontal and vertical TB data (TB_h fit and TB_v fit, respectively), resulting in 6 parameters describing the relation for SIT to horizontal and vertical TB, respectively. The modified fit is compared with the older intensity and polarization difference fits, which have been recalculated for the 53° incidence angle of CIMR. For the intensity fit, Equation (2.4) can be used; for the polarization difference fit, fit function (2.5) is used. The fit parameters of the new TB_h and TB_v fits, as well as the recalculated parameters for the I and Q fits, are shown in Table 2.2.

Table 2.2: Fit parameters for CIMR retrieval
Parameters for best fit of the trainings data for Equations (2.4) and (2.5). I and Q are recalculated at 53° incidence angle.

parameter	A	B	C	D
TB_h	74.527	217.795	21.021	-
TB_v	145.170	247.636	12.509	-
$I = (TB_v + TB_h)/2$	109.891	231.596	16.829	-
$Q = TB_v - TB_h$	71.086	34.322	38.731	2.142

The comparison showed that the TB_h and TB_v fits are very similar to the IQ fit. The $TB_v - TB_h$ fit even represents the increase of the polarization difference after the initial freeze-up, in the 5-10 cm range, which seems physically plausible, since the calming of seawater leads to a smaller sea surface roughness and thus to an increased polarization difference, better than the Q fit in the Q space (Huntemann & Spreen, 2022).

Other approaches to derive SIT are, for example, the methods of Gupta et al. (2019) or Paţilea et al. (2019). Gupta et al. (2019) retrieve thin SIT from SMOS TB polarization difference at 50° incidence angle and an empirical algorithm using only airborne SIT data for training. This method rejects the regions where the TB signatures of marginal SIC and thin SIT coincide and avoids the problem of distinguishing between the TB signatures of thin SIT and low SIC (Gupta et al., 2019). With the launch of SMAP in 2015, different approaches have been made to combine SMOS and SMAP data for a combined SIT product. For example, Paţilea et al. (2019) adapted the existing SMOS SIT retrieval from Huntemann et al. (2014) to SMAP by modifying the retrieval to use TBs at 40° incidence angle instead of averaging over the range of 40° to 50°, and by establishing a linear regression between the TBs at 40° incidence angle from SMOS and SMAP.

3 Data and Models

3.1 SMOS satellite data

The Microwave Imaging Radiometer using Aperture Synthesis (MIRAS) on board the European Space Agency's (ESA) Soil Moisture Ocean Salinity (SMOS) mission observes the Earth's global radiation at a relatively low microwave frequency of 1.4 GHz (λ = 21 cm), the so-called L-band. SMOS is designed to provide brightness temperature data in the L-band and to retrieve soil moisture and sea surface salinity fields in near real time (Balsamo et al., 2018). These microwave emissions from the Earth's surface can be used to map soil moisture and sea surface salinity, as well as sea ice thickness and other geophysical variables such as wind speed over the ocean and soil freeze-thaw conditions (ESA, 2017).

The SMOS satellite was launched in November 2009 and measures from a sun synchronous dusk-dawn polar orbit at an altitude of 757 km with an ascending (ascending half-orbit) equator crossing time of 06:00 LST (Local Solar Time) and a descending (descending half-orbit) equator crossing time of 18:00 LST (Balsamo et al., 2018; El Hajj et al., 2018; Huntemann et al., 2014). The MIRAS instrument is a passive microwave 2-D interferometric radiometer and has 69 receivers on three arms that measure radiances at 1.4 GHz, which due to interferometry is equivalent to a filled antenna of 8 m (Balsamo et al., 2018; Paţilea et al., 2019). The instrument measures the phase difference of incidence radiation, providing horizontal and vertical polarized brightness temperatures at incidence angles between 0° and 65°. MIRAS operates in a fully polarimetric mode, recording all four Stokes parameters. The large field of view allows for multi-angular observations organized into snapshots of approximately 1200 km × 1200 km (Paţilea et al., 2019). The SMOS footprint varies with the incidence angle from about 30 km × 30 km at nadir to 90 km × 33 km at about 65° (Huntemann et al., 2014). This scan configuration provides full daily coverage of latitudes between 50° and 86° (Kaleschke et al., 2012).

Although the frequency band near 1.4 GHz is not permitted for communications, radio frequency interference (RFI) does occur (Huntemann et al., 2014). And because a single RFI source on the Earth's surface contaminates the entire snapshot, since the synthetic aperture image reconstruction involves an inverse Fourier transformation**,** the snapshot is dismissed if at least one pixel has a TB greater than 300 K, since such high TBs are unrealistic in nature, so the TB is not affected (Huntemann et al., 2014; Kaleschke et al., 2012).

SMOS brightness temperature data are made available by ESA in several products. These include Level 1 products, which are intended for scientific and operational users who need to work with calibrated MIRAS instrument measurements, Level 2 soil moisture and ocean salinity products, which are intended for users who need to work with geo-located soil moisture and sea surface salinity estimates as retrieved from the L1 dataset, and Level 3 and 4 products, which include a wide range of products such as root zone soil moisture and drought index, L-band vegetation optical depth, thin sea ice or global rainfall estimates (Balsamo et al., 2018; ESA, 2017).

The Level 1B product contains the output of the image reconstruction of the SMOS observations. It consists of the Fourier components of the brightness temperatures in the antenna polarization reference frame at the top of the atmosphere (ESA, 2017).

The Level 1C brightness temperature product contains multi-incidence angle brightness temperatures at the top of the atmosphere, geolocated in an equal-area grid system, the Icosahedral Snyder Equal Area (ISEA) 4H9 grid (Paţilea et al., 2019). This is a hexagonal grid with a constant area of each cell and a non-uniform distance of approximately 15 km between the centers of two adjacent cells (Gupta et al., 2019).

In this thesis I will be working with gridded SMOS brightness temperature data on the National Snow & Ice Data Center's (NSIDC) Polar Stereographic Projection grid with a resolution of 12.5 km. This product originates from the University of Bremen and is operationally processed with SMOS Level 1C data version 7.24 as input. Older files saved before 2020 may have Level 1C 6.20 data as input because not all earlier SMOS data were reprocessed after the release of version 7.24. I will use SMOS brightness temperatures over a 10-year period obtained at an incidence angle of 53°, to match the CIMR incidence angle.

3.2 ERA5 data

ERA5 (Hersbach et al., 2023) is the fifth generation ECMWF reanalysis for the global climate and weather and is available from 1940 onwards. ERA5 provides hourly data of different quantities, such as eastward and northward component of the 10m wind, air temperature at 2 m above the surface, total column water vapor or sea ice area fraction. The spatial resolution is 0.25° x 0.25°. I used ERA5 data stored and downloaded at IUP of University of Bremen.

3.3 Cumulative Freezing Degree Days model

The Cumulative Freezing Degree Days (CFDD) model is an empirical model to calculate ice thickness growth under average snow conditions with only the air temperature as input (Bilello, 1961; Huntemann et al., 2014). It calculates the ice thickness by using negative daily average air temperatures to express the ice thickness growth:

$$SIT[cm] = 1.33 * (CFDD[°C])^{0.58} \tag{3.1}$$

Where CFDD is the integrated negative daily average air temperatures below the freezing point of seawater of -1.8 °C over the period since the first sea ice has been formed (Huntemann et al., 2014). SIT is the ice thickness, and the numbers are constants. This equation is a simplification of a more complex heat balance equation with a snow thickness (ST) of about (Petrich & Eicken, 2009):

$$ST = 0.08 * SIT \tag{3.2}$$

3.4 Thermodynamic energy balance model

The thermodynamic energy balance model used here is a modified version of the model of Tonboe (2005), Tonboe (2010). It uses ERA5 hourly data as input and calculates the surface energy balance. The model uses an adaptive Euler integration, which prevents major energy leaks by adjusting the time steps down to sub-second scale. It accounts for basic heat conduction and uses a thermal resistance approach for stabilization. In this sense, it is similar to the model of Kang et al. (2021). The salt transport for the initial freeze up and ice growth period includes the gravity drainage mechanism from Rees Jones and Worster (2013).

The model gives various output variables. The snow and ice thickness, the snow density, the ice salinity, the snow and ice average temperature and surface temperature for every timestep, as well as the temperature, density, thickness, exp correlation length, salinity and liquid water fraction for every single layer modeled during the timespan.

4 Method and Results

In this section I describe my methods and results of the analysis. I evaluate the new retrieval algorithm developed by Huntemann and Spreen for the CIMR mission by using a long time series of SMOS TB observations at L-band with 53° incidence angle for the initial ice growth phase up to thick first year ice in the Arctic and Antarctic. I will analyze the coefficients of the fit function (2.4) used to describe the dependence of TB on SIT. I will look for regional differences and for the consistency of these parameters with which SIT will be retrieved from CIMR TBs in the future. With two models I will try to separate the different physical effects contributing to the L-band signal, looking particular at ice thickness, snow depth and temperature.

To improve the amount of data used for the parameter estimation of the SIT retrieval, I need to use data from freeze up runs of different regions and years, to examine and remove the annual and regional dependence. For the analysis in the Arctic, I used L-band SMOS brightness temperatures at incidence angle 53° from October 1 to April 1 of the following year. This is because the retrieval only gives reasonable results for the for the initial ice growth phase up to thick first year ice during these months (Gupta et al., 2019; Huntemann et al., 2014). My analysis covers several years in the time span from 2011 to 2020. The regions I used for the analysis had to be selected to represent a continuous freeze up phase of first year ice from 0 % to 100 % sea ice concentration. The regions must not contain multiyear ice or sea ice cover at the beginning of the time series. They should have a continuous and relatively fast (1 month from 0 % to 100 %) growth of sea ice concentration, because then one can assume a homogeneous and continuous growth of sea ice thickness in this area. Furthermore, there should be no drops in sea ice concentration in the regions used, because these are possible break ups or melting events that make the parameter retrieval inaccurate and do not represent continuous freezing, and one simply doesn't know exactly what happens there afterwards. The regions used should also have less ice movement or drift, because then we would have SIT growth influenced by the drift of sea ice. Here I assume no strong drift in the areas used.

All of these conditions are required for the regions used in the analysis, because the fit function used later for parameter estimation can only represent a continuous increase in SIT, and drops in SIC would result in inaccurate parameter estimates and distort the dependence between SIT and TB.

I selected the regions for my analysis based on the criteria of continuous SIC growth from 0 % to 100 %. Using SIC maps during the freeze up phase of many years in the data browser of the University of Bremen, I selected five regions, shown in Figure 4.1, with three areas in each region. Figure 4.1 shows as an example the horizontal brightness temperature for the beginning of the freeze up season on October 1, 2020 on the left side and for the end on April 1, 2021 on the right side. The colors indicate whether open water or sea ice is present, as the

TB_h at 53° incidence angle is typically about 70 K for water and about 225 K for ice (cf. Figure 2.1). Therefore, blue represents open water and yellow represents sea ice. I used five regions, namely the Laptev Sea (A), Kara Sea (B), East Siberian Sea (C), Baffin Bay (D), and Beaufort Sea (G). In order to have a good amount of data for each region to work with, I selected three areas within each region. For the year 2020, almost every area meets the criterion of SIC evolution from 0 % to 100 % from the beginning to the end of the freezing season. I did not select regions in the northern Greenland Sea because the SIC was very variable due to the currents or storms. I also looked at Hudson Bay and the Chukchi Sea, but Hudson Bay had many data gaps and the Chukchi Sea has a high sea ice drift and a less homogeneous SIC.

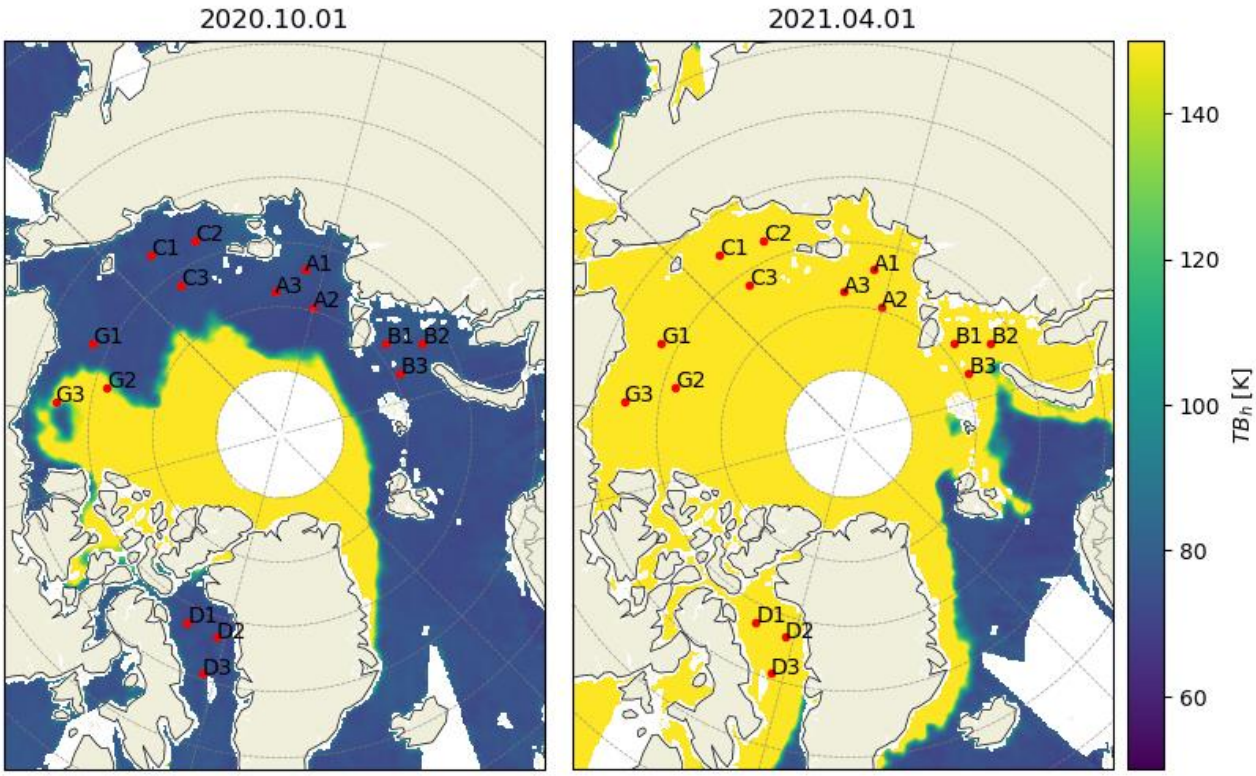

Figure 4.1: Selected regions in the Arctic
Arctic horizontal brightness temperature of 1.10.2020 (left) and 1.4.2021 (right) with red markers for the areas used in the analysis.

After selecting the regions, I selected only the freeze up runs with continuous SIC growth, without sea ice at the beginning and without sharp SIC drops during the freezing period. Figure 4.2 shows the ERA5 SIC for different freeze up runs in the Arctic in 2020. Areas G2 and G3 clearly show SIC at the beginning of the analysis period in 2020 and are therefore rejected. The SIC in area D2 shows a decrease in SIC of more than 60 % during the freeze up and is therefore also neglected. Only the areas with monotonic and sufficiently contiguous freeze up runs, such as the one from area C3, are used for further parameter estimation and analysis.

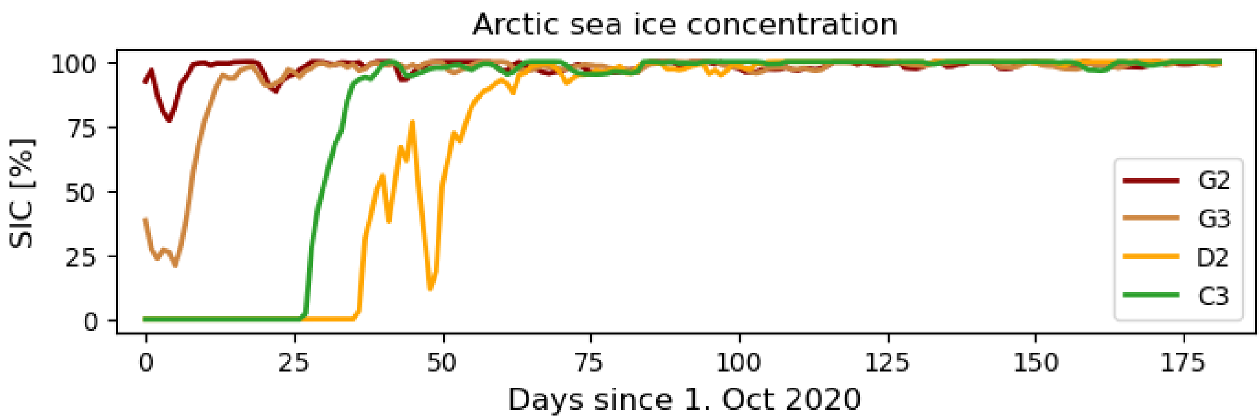

Figure 4.2: Arctic sea ice concentration runs
ERA5 SIC for four areas (C3, D2, G3, G2) in the Arctic from 1.10.2020 to 1.4.2021.

In total, I created a dataset of continuous freeze up runs for the initial ice growth phase up to thick first year ice from 15 areas in 5 different regions over 10 years. With this, I have significantly increased the dataset for training and parameter estimation compared to the currently used dataset in terms of spatial and temporal resolution. In the CIMR ATBD, they used freeze up runs of only one year in 2010 in 10 areas of the Kara and Barents Seas, which is more or less one region. Also, unlike my analysis, they did not manually select freeze up runs, but included every run in the analysis. Another difference is the time constraint of the freeze up runs. In my analysis, I examined TB evolution from October 1 to April 1 of the following year, while the CIMR ATBD only examines TB evolution through December 31.

The unprecedented data set examines and removes annual and regional dependencies, making the results of the analysis unique and significant.

Since I am extending the analysis to the Antarctic in this thesis to investigate whether the retrieval parameters can be used to represent the Antarctic, as well as to analyze differences between the Arctic and the Antarctic, I also selected regions based on previous criteria. It is more difficult to select regions with continuous SIC growth and no ice breakups in the Antarctic, because there is generally much more drift and movement in the Antarctic Sea than in the Arctic Sea. In addition, different ice growth processes occur in Antarctica, such as the formation of a snow-ice layer or the presence of sub-ice platelets, which further increase the ice thickness (Crocker & Wadhams, 1989). In areas where snow accumulates in large quantities, the resulting overburden pressure can lead to flooding of the ice surface and the formation of snow-ice (Crocker & Wadhams, 1989). Another process of ice growth is the contribution of the sub-ice platelets. They form when supercooled water comes into contact with the base of the ice sheet (Crocker & Wadhams, 1989). For the analysis, I chose three regions, namely the Ross Sea (A), the Weddel Sea (B) and at the coast of Dronning Maud Land

(C), with four areas in each region, as shown in Figure 4.3. As an example, Figure 4.3 shows exemplary the horizontal brightness temperature in Antarctica for the beginning of the freezing season on March 1, 2020 on the left and for the end on September 1, 2020 on the right. The time span I will analyze in Antarctica is from 2011 to 2021 from March 1 to September 1. I analyzed a total of 12 areas in 3 regions.

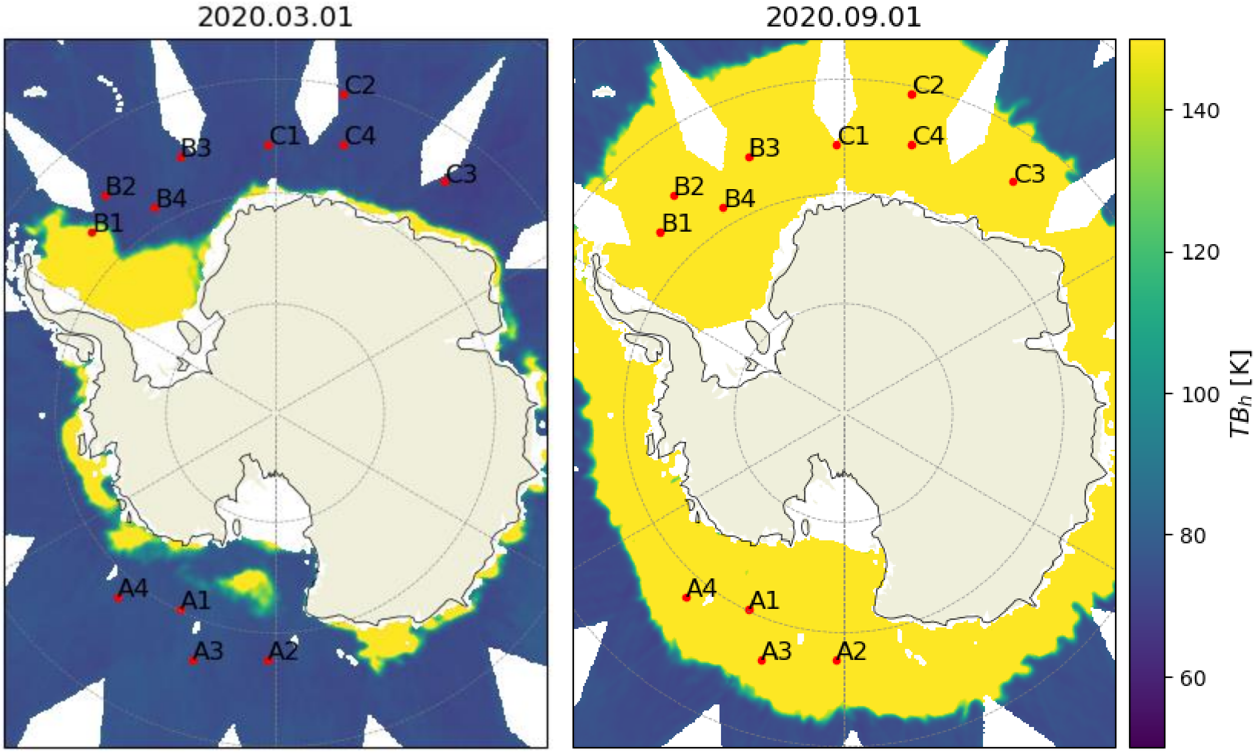

Figure 4.3: Selected regions in the Antarctic
Antarctic horizontal brightness temperature of 1.3.2020 (left) and 1.9.2020 (right) with red markers for the areas used in the analysis.

4.1 Sea Ice Thickness

To investigate the relation between TB and SIT for parameter estimation, I used modeled SIT from two different one dimensional models. The first one is the Cumulating Freezing Degree Days model (hereafter CFDD model) from Bilello (1961)**,** described in Section 3.3, which is used in Huntemann et al. (2014) and for training data for the CIMR retrieval method. I used this model for a better evaluation and comparison in the later analysis between the retrieval parameters estimated with my training dataset and with the training dataset of the CIMR ATBD. The CFDD model uses only air temperature as input. Using Equation (3.1) and the ERA5 2 meter temperature (T2m), I modeled the SIT evolution for all selected runs with continuous SIC growth.

The simple thermodynamic energy balance model (hereafter TD model), described in Section 3.4, is the second model I used to calculate SIT for the initial growth phase of first year ice. It models the ice and snow growth based on hourly ERA5 data and simple initial conditions for a starting situation of growing snow and ice layers. It produces the mean properties of snow and sea ice layers. The initial conditions for the sea ice growth are two layers. The upper layer is a 1 cm ice layer with a temperature of 269 K and a salinity of 22 ppt, and the lower layer is a 0.5 cm ice layer with a temperature of 270 K and a salinity of 8 ppt. The TD model gives many output variables (see 3.4) of which I use the snow and ice thickness of every timestep. It was convenient to use the model since the ERA5 data were already available. Figure 4.4 illustrates one model output for the area C3 in the Arctic in the year 2020. The model starts at the timestep where the SIC > 0 %. The dashed black line indicates the snow ice interface and one can see the temperature and thickness evolution of the sea ice and the snow. The grey and blue line represent the thickness of the snow and sea ice, respectively, further used in this thesis. The orange line shows the SIT evolution calculated with the CFDD model for the same area in the same year.

For the starting point of both models, I chose the point where the ERA5 SIC > 0 % in order not to miss information about thin sea ice in the training data, since, as noted in Huntemann et al. (2014)**,** SIC retrievals from current passive microwave algorithms yield ice concentrations below 100 % in the case of a thin ice cover. This means that the models start calculating ice thicknesses from the time the SIC starts to grow. Another reason for using the same starting point is to make the results more comparable, since both models have the same initial temperature conditions, and Huntemann and Spreen (2022) also included the initial increase in sea ice concentration in the training data.

The SIT evolution between these two models shows clear differences. In general, the CFDD modeled SIT evolution is slower and has lower end thicknesses in all regions (not shown) compared to the TD modeled SIT. Figure 4.4 shows a case where the snow cover is particularly low, so the difference is expected in this case. A general overestimation of sea ice thickness by the TD model may be an effect of the choice of parameters for the model runs.

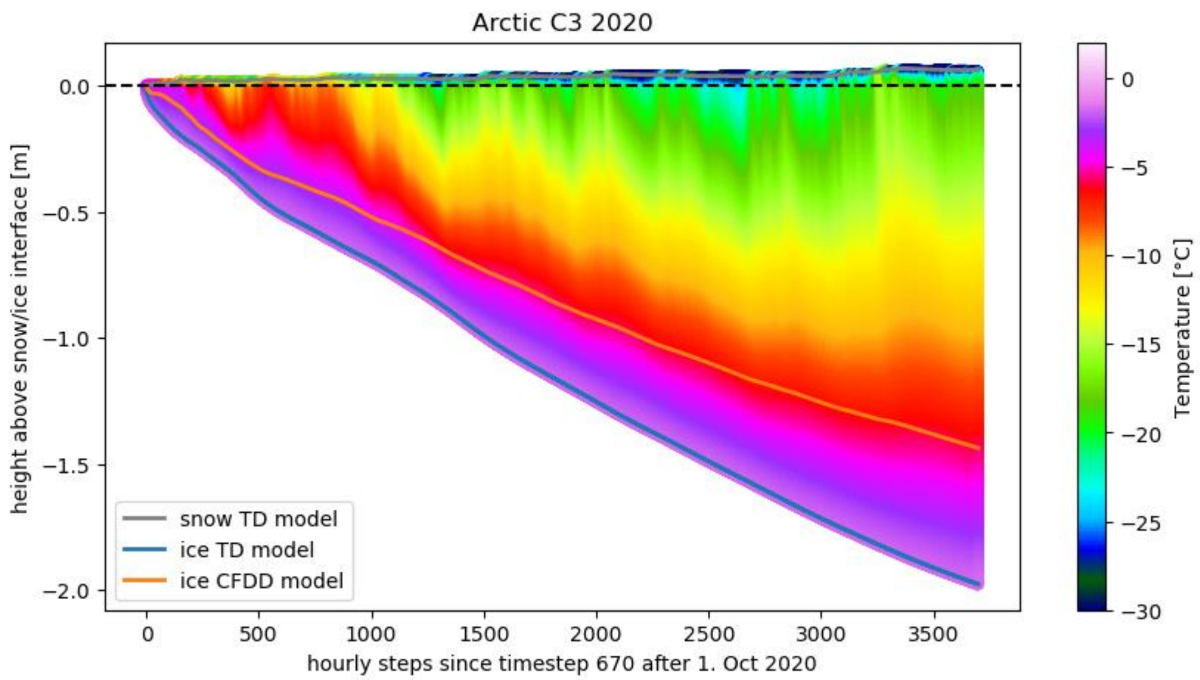

Figure 4.4: Thermodynamic energy balance model output
TD model output for area C3 in 2020 in the Arctic. Dashed black line indicates the snow ice interface. The grey and blue line indicate the TD model snow and ice thickness, respectively. The orange line represents the ice thickness calculated with the CFDD model.

The fundamental difference between these two models is the treatment of snow growth. Although snow has no direct effect on the measured TB at L-band because snow is nearly transparent at this frequency, it has a thermodynamic warming effect that affects the temperature and thus the TB (Huntemann et al., 2014). While the CFDD model uses only temperature as input and assumes 8 % of the ice thickness as snow thickness as an average condition in the Arctic (Bilello, 1961; Huntemann, 2015), the TD model simulates the snow growth separately based on different parameters as it uses much more atmospheric input data. Therefore, the TD model is expected to provide a much better representation of snow growth because it does not make general assumptions, but is modeled with local atmospheric parameters. The use of the TD model is especially interesting for snow thicknesses in Antarctica, because the CFDD model simulates snow as an average condition in the Arctic and Antarctica typically has more snowfall, which means that the TD model could better represent the snow for the Antarctic. In Section 4.4 I will take a closer look at the dependence of snow on TB.

It should be noted that both models can only simulate normal ice growth and do not take into account flooding or other ice growth processes, such as the formation of a sub-ice platelets layer. However, this mainly concerns the SIT in Antarctica, as such events are rare in the Arctic. Therefore, results from Antarctica must be treated with extra caution, as it is dangerous to assume that models that tend to accurately predict ice growth in the Arctic will also accurately predict ice growth in Antarctica.

4.1.1 TB and SIT relation

The dependence of the L-band TB on the SIT is the relation used in many studies for SIT retrieval, for example in Huntemann et al. (2014), Kaleschke et al. (2012) and Paţilea et al. (2019). The correlation of ice thickness with air temperature, and thus surface temperature, was found to be the main reason for the relation between ice thickness and brightness temperature (Huntemann, 2015). Figure 4.5 shows an example of the relation between the horizontal and vertical SMOS TB at 53° incidence angle and the modeled SIT from the CFDD model of 2020. Different regions can be identified by the color. The TB_h, indicated by circles, shows lower brightness temperatures, slower increase and later saturation with SIT than the TB_v, but is generally subject to more noise. The TB_h has much more variability even at higher ice thicknesses, while the TB_v is much more stable. The characteristics of TB_h and TB_v shown in Figure 4.5 are generally in line with expectations (Huntemann, 2015).

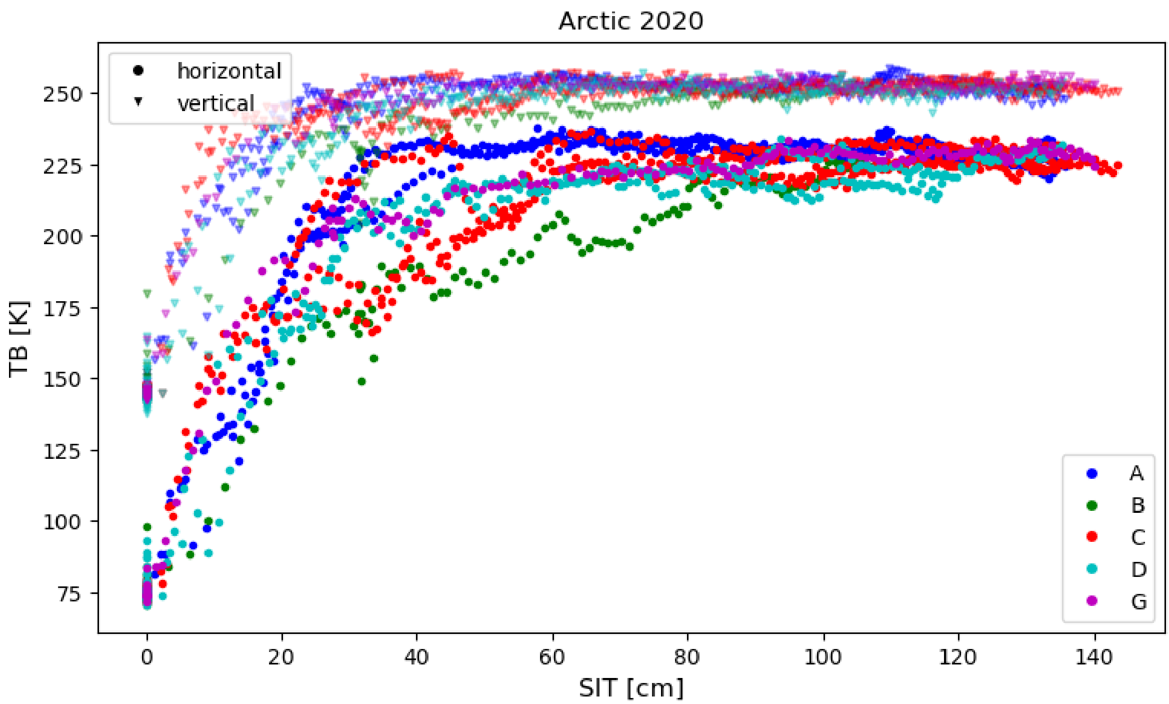

Figure 4.5: Arctic sea ice thickness against brightness temperature
SIT from CFDD model against SMOS TB at 53° incidence angle for the Arctic in 2020. Colors indicate different regions, symbols indicate horizontal and vertical brightness temperatures.

4.2 Fit parameter

To analyze the relation between SIT and TB at L-band, I used the same method as in the CIMR ATBD and fit the same analytical Equation (2.4) to the newly obtained data set, which can be described as a forward model where the coefficients are determined empirically, to perform a least squares fit on TB and SIT (Huntemann & Spreen, 2022). The retrieved parameters can then be used by inverting the forward model and retrieving the SIT from the TBs by minimizing the differences weighted with all known errors weighted again and summed up in a cost function. The parameters A (brightness temperature of open water close to sea ice under freezing conditions), B (brightness temperature of thick sea ice) and C (a curvature parameter connecting the two TBs) are denoted with h and v as the index for the TB_h fit and TB_v fit, respectively. Fitting and parameter estimation are performed under the assumption that the TBs and the ice thicknesses of both models are true.

With many more regions and years, manually selected freeze up runs, a longer timespan of the freezing period and two different models to model the SIT growth, I examine differences in parameters between regions, years and models and compare them to the values of the CIMR ATBD. Additionally, I will investigate the fit parameters for the Antarctic and compare them to the Arctic.

To analyze and compare the fit parameters, I performed the parameter retrieval for each individual freeze up run with modeled SIT from both models. An example plot is shown in Figure 0.1 in the Appendix for the 2018 freeze up run for area A1 with modeled SIT from the CFDD model. I also stepped through each fit plot and examined outliers. Outliers are mainly caused by the misrepresentation of the relation between TB and SIT in the first few centimeters of SIT, where the model has not calculated SIT, but TB is increasing. This has the effect that at 0 cm SIT the TB reaches its tie point for the TB of thick ice (parameter B), causing the parameter C to approach zero. These runs are then excluded for further comparison.

The parameters determined for the CIMR SIT retrieval by Huntemann and Spreen, which describe the relation for SIT to horizontal and vertical TB, respectively, can be found in Table 2.2 and are used for comparison with my analysis.

4.2.1 Arctic

Figure 4.6 shows the three fit parameters obtained from all the Arctic freeze up runs as histogram plots. The blue histogram denotes the parameters for the TB_h fit and the red one for the TB_v fit. On the left the fit parameters are calculated with SIT from the CFDD model, on the right with SIT from the TD model. The thick line represents a kernel density estimate (KDE), which visualizes the distribution of the data using a continuous probability density curve. The mode of this distribution is indicated by a thick dashed line and a bold number. The dotted line with the thin number indicates the parameter values from the CIMR ATBD (Huntemann & Spreen, 2022).

The basic features and differences of the distributions compared to the parameters from the CIMR ATBD are clearly visible. For parameters A and B, the parameter retrievals from both models yield very similar distributions and values, although the mode of the distribution differs from the CIMR ATBD values. For parameter A the difference is very small with 1 K to 2 K for both TB_h and TB_v fits and for both models. For parameter B, the difference is much larger. The value of the mode for both models is about 11 K higher for the TB_h fit and about 5 K higher for the TB_v fit than the CIMR ATBD values. The mode of parameter A seems to be in good agreement with the CIMR ATBD values, while the CIMR ATBD value of parameter B is lower than the mode of the distribution for both fits and both models. This may be explained by the longer freeze up period (Oct. 1 to Apr. 1) used for my data set. Since both models give very similar results, it may be that the tie point for thick sea ice (B) is not reached for the fit function with the shorter period (Oct. 1 to Dec. 31) of the CIMR ATBD, but can be determined with the longer period. Another reason could be the influence of another variable such as snow thickness, which leads to higher TB through a increase of emissivity, which I will discuss in Section 4.4. For the parameter C, there are significant differences from the CIMR ATBD values. The mode of the parameter distribution is lower for both fits of the CFDD model and higher for both fits of the TD model compared to the CIMR ATBD values. The difference between the models can be explained by the different ice growth rates in the models. Because the SIT from the TD model results in higher total thicknesses at every timestep, the fit curve, and therefore the relation between SIT and TB, has less curvature, since the same TB is compared to different SITs from models. Therefore, a lower parameter C results in a higher curvature of the fit line, which results in a lower SIT retrieval for the same TB. A higher parameter C results in a lower curvature of the fit line, resulting in a higher SIT retrieval for the same TB. The difference of the C parameter to the CIMR ATBD values is discusses further in Chapters 5 and 6. Altogether, each parameter value derived with the CFDD modeled SIT is closer to the parameter values of the CIMR ATBD than the parameters obtained with the SIT from the TD model. This may be because the CFDD model is also used in the CIMR ATBD to generate SIT training data.

Overall, Figure 4.6 shows that the distributions of the parameters more or less follow a Gaussian distribution, and that parameters B and C in particular show differences for different data sets and models used. The wider distribution of the parameters from the TB_h fit to the TB_v fit, can be explained by the variability of the horizontal and vertical polarized TB. As described in 4.1.1, the TB_h is much noisier than TB_v and has a higher variability, resulting in a wider distribution of the brightness temperature of thick sea ice.

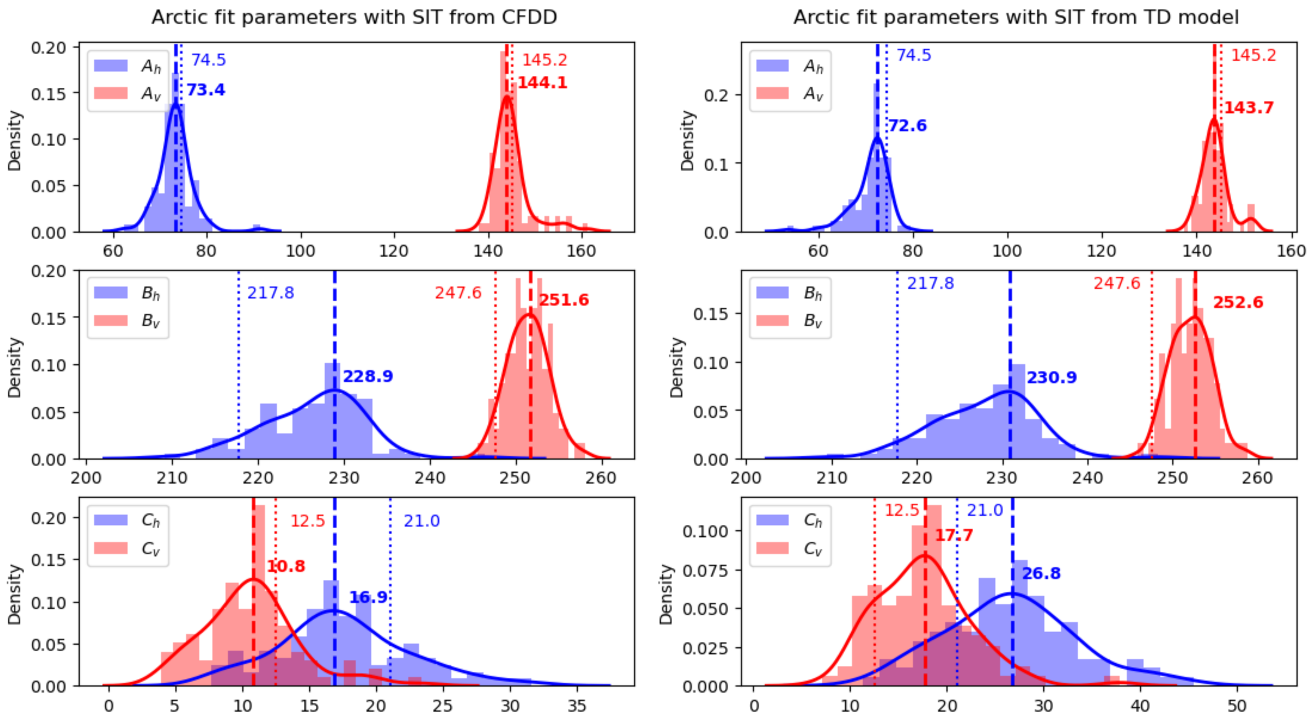

Figure 4.6: Arctic fit parameters with SIT from CFDD and TD model
Fit parameters for all runs in the Arctic for years 2011-2020 as histogram with modeled SIT from the CFDD model (left), and from the TD model (right). Dotted line represents ATBD parameter values. Dashed line represents mode of KDE (Kernel density estimation).

4.2.2 Arctic regional differences

In this section, Arctic regional differences in fit parameters are analyzed and compared with CIMR ATBD values (Huntemann & Spreen, 2022). First, I will look at the fit parameters derived with SIT calculated with the CFDD model. Figure 4.7 shows the retrieved fit parameters of the TB_h and TB_v fits for region B in the Arctic as histogram plots. Although region B in the Kara Sea is close to the original training areas for the CIMR ATBD parameters, the modes of the B and C parameter distributions, denoted by a thick dashed line and a bold number, differ from the values of the CIMR ATBD parameters (dotted line) in the same way as the modes in Figure 4.6. The same differences in the distribution modes of one region and of the whole Arctic to the CIMR ATBD values raise the question of whether all regions result in the same parameter distribution when considered separately, and whether there are regional differences.

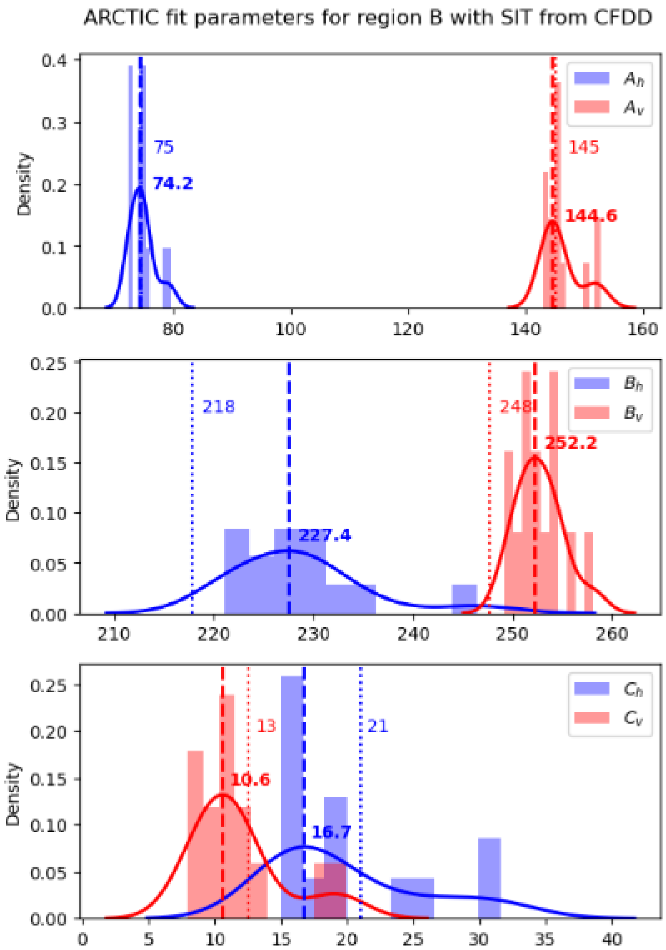

Figure 4.7: Arctic fit parameters for region B with SIT from CFDD model
Fit parameters for runs in the Arctic in region B for years 2011-2020 as histogram with modeled SIT from the CFDD model. Dotted line represents ATBD parameter values. Dashed line represents mode of KDE (Kernel density estimation).

To compare the five different regions in the Arctic, I looked at the mean and standard deviation of the parameter distributions. These are shown in Table 4.1. The CIMR ATBD parameters are also included for quick comparison. The blue numbers indicate that the CIMR

ATBD parameter is within the range of the mean ± one standard deviation in that region, and the red numbers indicate that it is outside the range.

Table 4.1 shows that the value of the C parameter for the TB_h fit is always higher than for the TB_v fit. This is plausible because, as described in Section 4.1.1, TB_h has a slower increase and later saturation with SIT than TB_v, resulting in a lower curvature of the fit curve and a higher parameter C. The higher values of the standard deviations of the parameters B and C for the TB_h fit than for the TB_v fit can be explained by the higher variability of TB_h for thick ice, which causes a higher variability in the parameter B and in the curvature of the fit line.

The values of parameter A are very stable in all five regions of the Arctic and show no large regional differences. All values and the obtained CIMR ATBD parameter are within one standard deviation of each other. The mean values of parameter B are within one standard deviation of each other and also show no regional differences, except for region D. This is the only region where the CIMR ATBD value is within one standard deviation of the mean value of the distribution. The overall value of the mean is about 11 K and 5 K higher than the CIMR ATBD value, for B_h and B_v respectively, excluding region D. This is the same difference as found in Figure 4.6. The mean of the C parameter is lower than the CIMR ATBD parameter for almost all regions for C_h and C_v, but has the highest regional variability of all parameters. However, due to the high standard deviation, which is about $\frac{1}{4}$ to $\frac{1}{3}$ of its parameter value, the regional differences are small compared to the overall variability. Parameter C probably has the highest regional and overall variability because it is most influenced by the relation between TB and SIT, which contains a lot of variability, and parameters A and B because it describes the curvature of the fit line.

Overall, the regional differences of the parameters are small compared to the overall variability and cannot be detected for the parameters. Parameter A shows a high correlation with the CIMR ATBD value, while parameter B has an offset to the CIMR ATBD value and parameter C shows high regional differences but also high variability and is most influenced by the relation of TB to SIT. Only for region D are all CIMR ATBD parameters within the range of one standard deviation, which raises the question of whether region D and the CIMR ATBD training area are similarly influenced by some other variable such as snowfall, or whether region D is just an outlier since it is only one region out of five. This is discussed further in Section 4.4.

Table 4.1: Arctic parameter mean and standard deviation (CFDD)
Mean and standard deviation for fit parameters of different regions in the Arctic retrieved with SIT from the CFDD model.

	ATBD	Region A	Region B	Region C	Region D	Region G
A_h	74.527	72.6 ± 3.8	74.7 ± 2.1	74.8 ± 5.3	73.0 ± 2.5	72.0 ± 3.0
A_v	145.170	145.8 ± 3.9	146.2 ± 3.3	146.6 ± 5.6	143.3 ± 2.2	143.6 ± 2.3
B_h	217.795	229.5 ± 2.9	228.5 ± 6.7	229.6 ± 3.6	219.7 ± 4.3	227.6 ± 3.7
B_v	247.636	251.2 ± 1.3	252.7 ± 2.4	252.8 ± 1.8	248.9 ± 1.5	253.3 ± 1.5
C_h	21.021	16.6 ± 3.4	19.9 ± 5.7	15.9 ± 5.1	19.2 ± 4.2	16.0 ± 5.6
C_v	12.509	9.8 ± 2.7	11.8 ± 3.5	8.2 ± 2.6	12.7 ± 3.5	10.3 ± 3.7

Although the regional differences were found to be small with the SIT training data from the CFDD model, I will now evaluate the fit parameters derived with the SIT calculated with the TD model. I compare them to the CFDD and CIMR ATBD parameters and examine the regional differences, also because the TD model uses a different method to simulate ice thickness growth with more input data in each region, as well as separate snow growth. The mean and standard deviation of the parameter distributions of the five different regions in the Arctic are shown in Table 4.2. Again, the blue numbers indicate that the CIMR ATBD parameter value is within the range of the mean ± one standard deviation in that region. Red numbers indicate that the CIMR ATBD parameter is outside the range of one standard deviation.

The parameter A is again very stable in all regions and all values are within one standard deviation of each other. Nevertheless, the mean value of the distribution shows a larger difference of 2 K to 4 K for A_h to the CIMR ATBD value for each region for the TB_h fit and is also lower than the mean value of the parameter A_h obtained with the CFDD modeled SIT. The parameter A_v shows such differences only in regions D and G. The parameter B again shows no regional differences except for region D where the value is again closest to the CIMR ATBD value. The mean values of parameter B again show much higher values compared to the CIMR ATBD values as in Table 4.1, but are 1 to 2 K higher than the B parameter values for the CFDD model. The mean of the C parameter distribution for each region is higher compared to the CIMR ATBD values, as can also be seen in Figure 4.6, but except for region B and D, the CIMR ATBD parameter C is within the variability range of one standard deviation. However, as the standard deviation is again high compared to the parameter value, the regional differences are again small.

The mean values of the distributions in Table 4.2 show overall the same characteristics and no regional differences as above, however parameter A has slightly lower, parameter B has slightly higher and parameter C much higher values than the CIMR ATBD values.

Table 4.2: Arctic parameter mean and standard deviation (TD)
Mean and standard deviation for fit parameters of different regions in the Arctic retrieved with SIT from the TD model.

	ATBD	Region A	Region B	Region C	Region D	Region G
A_h	74.527	70.5 ± 4.2	72.6 ± 2.6	70.9 ± 5.1	72.0 ± 2.4	70.0 ± 4.0
A_v	145.170	144.7 ± 3.4	145.0 ± 2.8	144.6 ± 2.9	142.8 ± 2.1	142.5 ± 2.4
B_h	217.795	230.7 ± 3.0	230.9 ± 6.9	231.2 ± 4.0	221.5 ± 4.8	229.0 ± 3.8
B_v	247.636	251.7 ± 1.3	253.5 ± 2.5	253.4 ± 1.8	249.6 ± 1.7	253.9 ± 1.5
C_h	21.021	245.0 ± 4.8	29.0 ± 6.6	24.7 ± 6.7	29.0 ± 6.8	24.8 ± 8.3
C_v	12.509	16.2 ± 3.9	18.4 ± 3.5	15.0 ± 3.7	20.2 ± 5.6	17.2 ± 5.1

4.2.3 Antarctic

I am now using the data set created for the Antarctic and both models to derive the fit parameters of the Antarctic freeze up runs. I am investigating whether the retrieval parameters from the Arctic can be used to represent the fit parameters of the Antarctic, and I am analyzing the differences between the parameters in the Arctic and the Antarctic. Again, the modeled SIT should be viewed with caution, as both models can only simulate normal ice growth.

The three fit parameters retrieved from all Antarctic freeze up runs are shown as histogram plots in Figure 4.8. On the left, the fit parameters are calculated with SIT from the CFDD model, and on the right, with SIT from the TD model. The blue and red histograms indicate the parameters for the TB_h and TB_v fits, respectively. The dotted line with the thin number now indicates the value of the mode of the Arctic parameter distribution for the CFDD model on the left and the TD model on the right.

First, the A and B parameters show pretty much the same mode values for the fit parameter distributions derived with SIT from different models. As in the Arctic, the mode of the B parameter distribution of the TD model has slightly higher values compared to the CFDD model. Only the C parameters again show the greatest differences between the two models, but have the same tendency for higher parameter values with SIT from the TD model. Furthermore, the comparison of the mode values of the parameter distributions between the Antarctic and the Arctic, where the dotted line indicates the mode of the Arctic parameters, shows that for the parameters A_h and B_h the differences between the Arctic and the Antarctic parameters are small for both models, whereas for the parameters A_v and B_v the differences between the Arctic and the Antarctic parameters are twice as large for both models compared to the A_h and B_h differences. However, the differences between Arctic and Antarctic are smaller for C_v than for C_h. For both models, the Antarctic curvature parameter C is smaller than for the Arctic one, which means that the fitted curve has a higher curvature and that both models model slower ice thickness growth for the Antarctic than for the Arctic, assuming the same dependence of SIT on TB. However, because the C parameter is higher for the TD model than for the CFDD model, the TD model also models higher ice thicknesses in the Antarctic than the CFDD model.

Overall, the same features appear for the Antarctic when comparing the CFDD with the TD model as for the Arctic. The parameters A and B show good similarities to the values of the Arctic, but especially for the parameter B_v it would be interesting to investigate why the difference between Arctic and Antarctic is twice as large as the difference in B_h, since TB_v is typically much less variable than TB_h. The C parameter indicates slower ice growth in Antarctica than in the Arctic of both models.

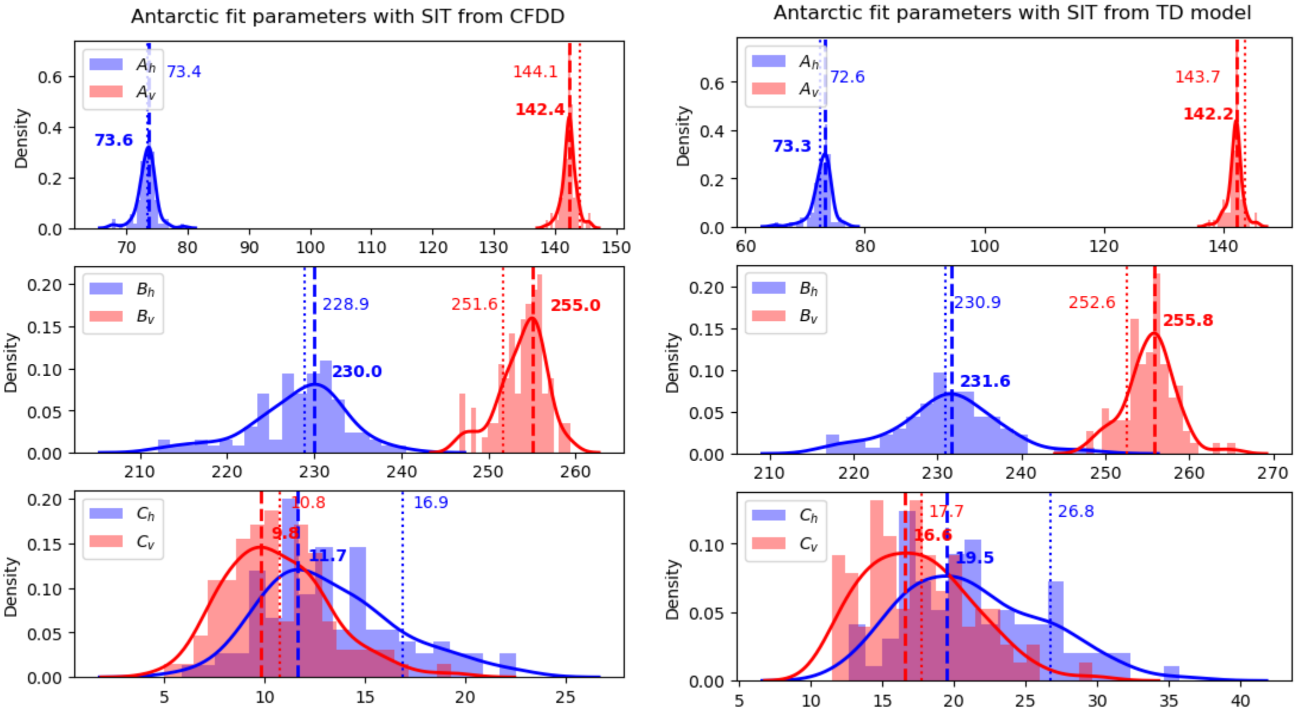

Figure 4.8: Antarctic fit parameters with SIT from CFDD and TD model
Fit parameters for all runs in the Antarctic for years 2011-2021 as histogram with modeled SIT from the CFDD model (left), and from the TD model (right). Dotted line represents Arctic parameter values. Dashed line represents mode of KDE (Kernel density estimation).

4.2.4 Antarctic regional differences

In this section, I compare the fit parameters from three different regions of Antarctica and look at the regional differences. Table 4.3 and 4.4 show the mean and standard deviation of the parameter distributions for the CFDD and TD models, respectively.

For both models, the parameter A has very small standard deviations and almost no differences at all. The mean values of parameter B have slightly higher values for the TD model, but region A shows a difference of about 5 K for B_h and 3 K for B_v compared to the other two regions for both models. Parameter C values are higher for the TD model compared to the CFDD model as shown in Figure 4.8, but region C shows significant higher values for both models while the other two regions show very similar values.

Overall, there is no regional difference in the parameters A, B and C estimated with SIT from both models. However, parameter B in region A and parameter C in region C show significant regional differences that that could be further investigated, e.g. with respect to regional changes in heat flux.

Table 4.3: Antarctic parameter mean and standard deviation (CFDD)
Mean and standard deviation for fit parameters of different regions in the Antarctic retrieved with SIT from the CFDD model.

	Region A	Region B	Region C
A_h	73.7 ± 1.4	72.9 ± 2.2	73.3 ± 0.8
A_v	142.6 ± 1.2	142.0 ± 1.4	142.5 ± 0.6
B_h	224.6 ± 4.2	230.9 ± 2.6	229.2 ± 6.9
B_v	252.3 ± 2.4	255.4 ± 1.1	253.9 ± 3.4
C_h	11.8 ± 2.5	12.5 ± 2.6	16.0 ± 3.6
C_v	9.8 ± 2.5	9.8 ± 1.7	12.5 ± 2.6

Table 4.4: Antarctic parameter mean and standard deviation (TD)
Mean and standard deviation for fit parameters of different regions in the Antarctic retrieved with SIT from the TD model.

	Region A	Region B	Region C
A_h	73.4 ± 1.5	72.0 ± 2.1	73.1 ± 0.8
A_v	142.3 ± 1.3	141.5 ± 1.4	142.3 ± 0.6
B_h	228.0 ± 5.0	232.9 ± 3.1	233.8 ± 8.5
B_v	253.9 ± 2.7	256.4 ± 1.5	256.0 ± 4.3
C_h	19.7 ± 4.3	20.2 ± 4.0	25.9 ± 4.3
C_v	16.7 ± 4.1	16.4 ± 2.9	20.4 ± 3.0

4.2.5 Arctic and Antarctic temporal evolution

With the much longer timespan of my data set, it is possible for the first time to look at the temporal variability and analyze if there is a temporal evolution of the retrieved parameters.

In Figure 4.9 the three fit parameters from all freeze up runs of the TB_h (blue) and TB_v (red) fits for the Arctic are sorted by the years 2011 to 2020. On the left the SIT is calculated with the CFDD model, on the right the SIT is calculated with the TD model. The black line connects the mean of the distributions for each year. The dashed line represents the trend line of the annual means, and the number indicates the slope of the line.

The mean values of the parameters A_v, A_h and B_v show no significant changes over the 10 year period for both models. Although the annual means of A_h from the TD model show a slight positive trend of 0.23, which could be due to the selection of a suboptimal starting point for the model. It can be neglected due to the high overall stability of this parameter. The annual means of the parameter B_h show more variability between years, with a trend of > 0.2 for both models, but compared to its overall variability and because the parameter could be influenced by snow thickness, the variability between years is not significant. Furthermore, there is no continuous change in one direction and perhaps with a longer timespan the now slightly positive trend would flatten out. The annual means of parameter C vary much more than B_h, but are also subject to much more noise. Only the annual means of the C_h parameter for the CFDD model show a temporal evolution that could be significant. However, the trend in a highly variable parameter must be viewed with caution and will be discussed in Chapter 6.

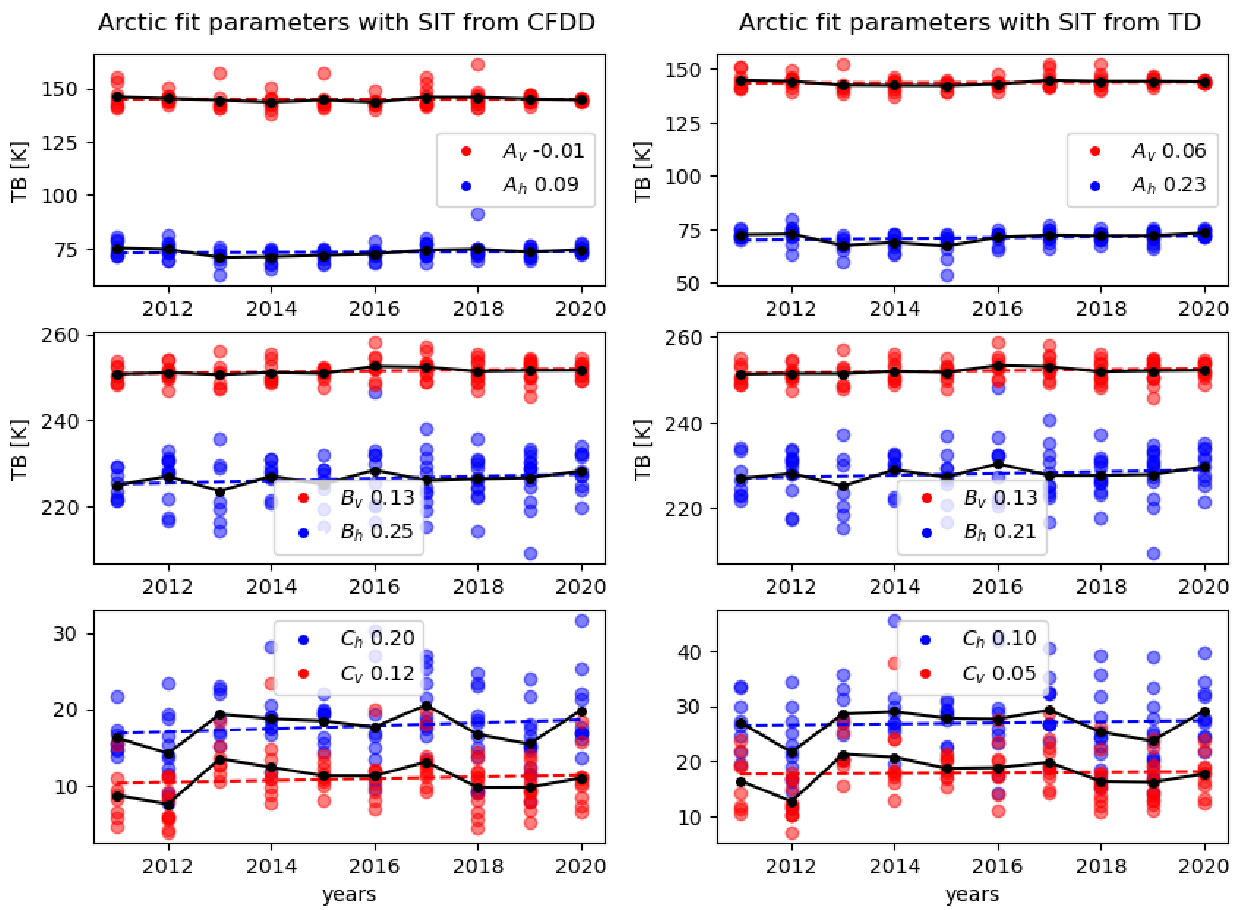

Figure 4.9: Temporal evolution of Arctic fit parameters
Fit parameters for all runs in the Arctic sorted by years 2011-2020 with modeled SIT from the CFDD model (left), and from the TD model (right). Black dots represent the mean of each year. Dashed line represents the trend line of the annual means and the number indicates the slope of the line.

For the analysis of temporal evolution of the fit parameters in Antarctica, Figure 4.10 shows the parameters from all freeze up runs sorted by the years 2011 to 2021, with the SIT calculated with the CFDD model on the left side and the SIT calculated with the TD model on the right. No ERA5 data were available on the server at time of processing for the year 2016. The annual mean for this year is the mean of the years 2015 and 2017.

In the Antarctic, the annual means of the parameters A_v, A_h and B_v again show no changes or temporal evolution over the 11 year period for either model. The parameter B_h shows a small trend in the annual means for both models, but as for the Arctic, it is not that significant and may be influenced by to the low mean value of 2011. The parameter C again shows a positive temporal evolution for both fits and models, with the annual means of the parameters of the horizontal fits being slightly higher than those of the vertical fits. Although parameter C has a high variability, the trend of the annual means shows a significant positive trend for both models in Antarctica.

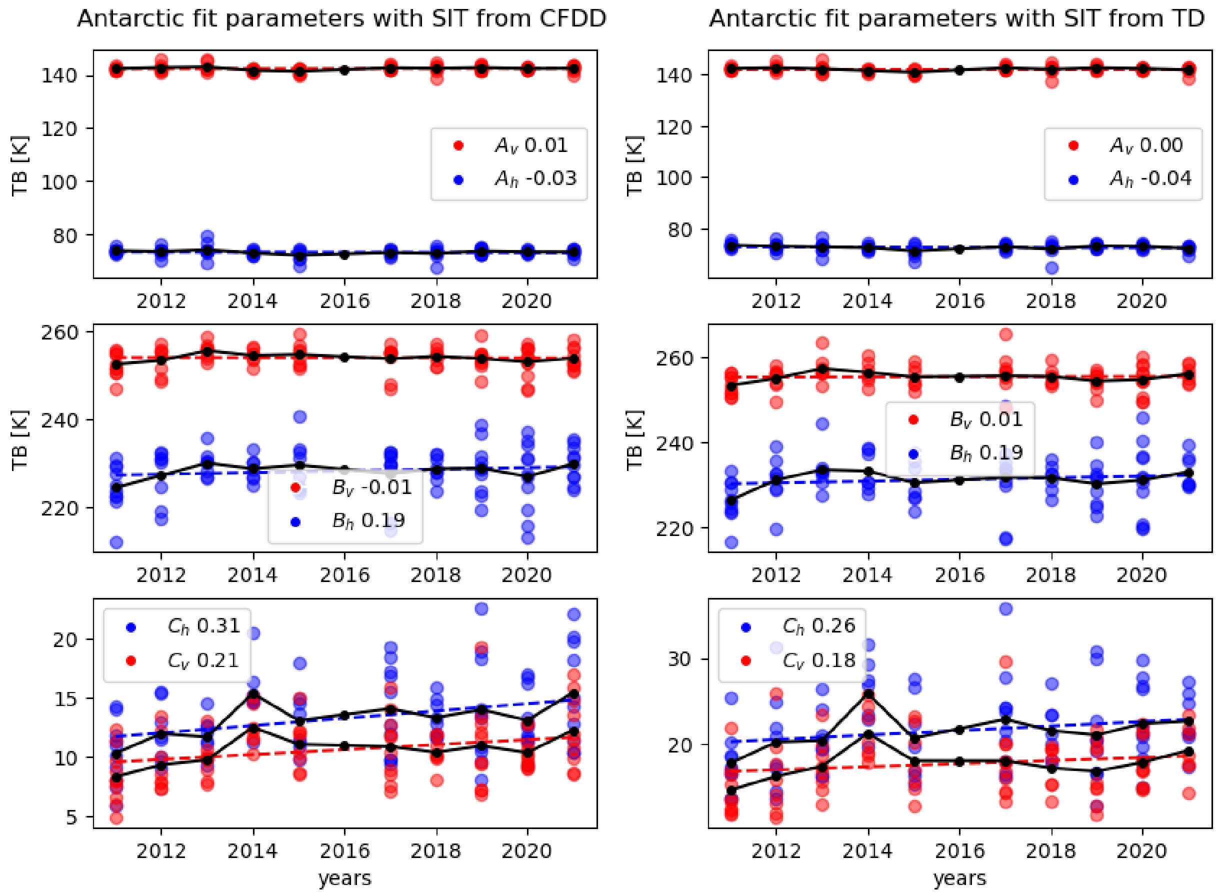

Figure 4.10: Temporal evolution of Antarctic fit parameters
Fit parameters for all runs in the Antarctic sorted by years 2011-2021 with modeled SIT from the CFDD model (left), and from the TD model (right). Black dots represent the mean of each year. Dashed line represents the trend line of the annual means and the number indicates the slope of the line.

4.3 Sensitivity analysis

In this section I conduct a sensitivity study. I am investigating the sensitivity of the TB to changes in SIT for both models used in the Arctic and the Antarctic. I investigate this because how much the TB is sensitive to a change in SIT gives an idea of the invertibility for the later retrieval. To analyze the sensitivity of TB to changes in SIT, I used the derivative of the fit function, Equation (4.1):

$$f'(x) = \frac{(B - A) * exp(-x/C)}{C} \tag{4.1}$$

Where A, B and C are the parameters and x is the SIT. The criterion for when TB is sensitive to a given SIT change is, for my analysis, when the slope of the fit function is 1/25. This means that a 1 K change in TB will propagate into a 25 cm change in ice thickness. I chose this criterion under the assumption that the satellite accuracy of the measured TB is 1 K, although Wu et al. (2013) report an even higher accuracy. For the SIT, I allow a maximum error of 25 cm as an uncertainty factor for the ice thickness.

I repeated the sensitivity analysis for each freeze up run in the Arctic and Antarctic and compared it with the calculated sensitivity of the CIMR ATBD parameters, which is 108 cm and 87 cm for the TB_h fit and TB_v fit, respectively, which will be used for comparison.

4.3.1 Arctic

The sensitivities of TB to changes in SIT for both models from all Arctic freeze up runs are shown as histogram plots in Figure 4.11. The blue histogram denotes the sensitivities for the TB_h fit and the red one for the TB_v fit. On the left the sensitivity is calculated with SIT from the CFDD model, on the right with SIT from the TD model. The thick line represents a kernel density estimate (KDE), which visualizes the distribution of the data using a continuous probability density curve. The mode of this distribution is indicated by a thick dashed line and a bold number. The dotted line with the thin number indicates the sensitivity values calculated with the parameters from the CIMR ATBD (Huntemann & Spreen, 2022).

For both models the sensitivity histogram of the TB_h fit has a wider distribution than the TB_v fit, which is due to the higher variability in all parameters. The sensitivity values with SIT from the CFDD model are lower than the sensitivities with SIT from the TD model, which is due to the lower C parameter for the CFDD model. The sensitivity is strongly dependent on C, because the degree of curvature affects the slope of the fit function. The sensitivities from the CFDD model for both fits are lower than the CIMR ATBD values because the C parameter is also lower, while the sensitivities from the TD model are higher. Overall, the sensitivity of the CFDD model is closer to the CIMR ATBD values with 108 cm and 60 cm for the TB_h and the TB_v fits, respectively, than the sensitivities from the TD model, probably because the same model is used as for the CIMR ATBD values and therefore the rate of SIT growth is similar.

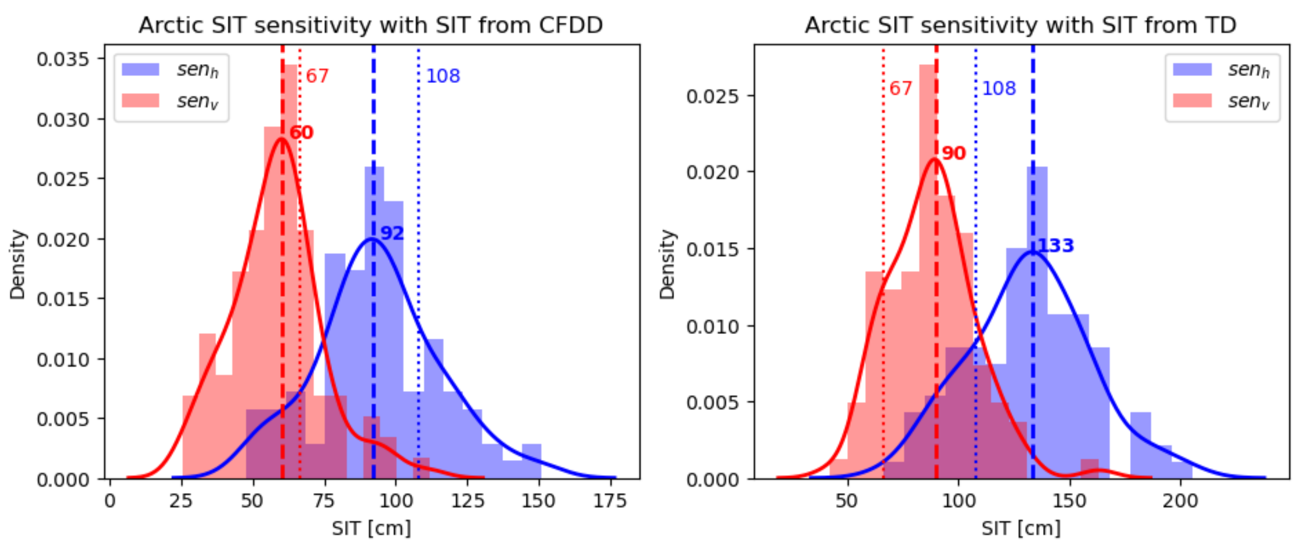

Figure 4.11: Arctic sensitivity histogram of all runs
Histogram of SIT sensitivities for parameter fits in the Arctic with SIT from the CFDD model (left) and the TD model (right). Dotted line represents CIMR sensitivity values. Dashed line represents mode of KDE (Kernel density estimation).

4.3.2 Antarctic

The sensitivities of TB to changes in SIT for both models from all Antarctic freeze up runs are shown as histogram plots in Figure 4.12. The dotted line with the thin number now shows the sensitivity values from the Arctic for the different models.

For both models, the Antarctic sensitivities are lower than the Arctic sensitivities due to the lower C parameters and therefore higher curvature of the fit curve, the criterion being reached at lower SIT values.

The Arctic and Antarctic have clearly different sensitivities. The Antarctic fits may be less reliable, because the upper tie-point for thick ice is usually not reached, but the fit curve still has a curvature there.

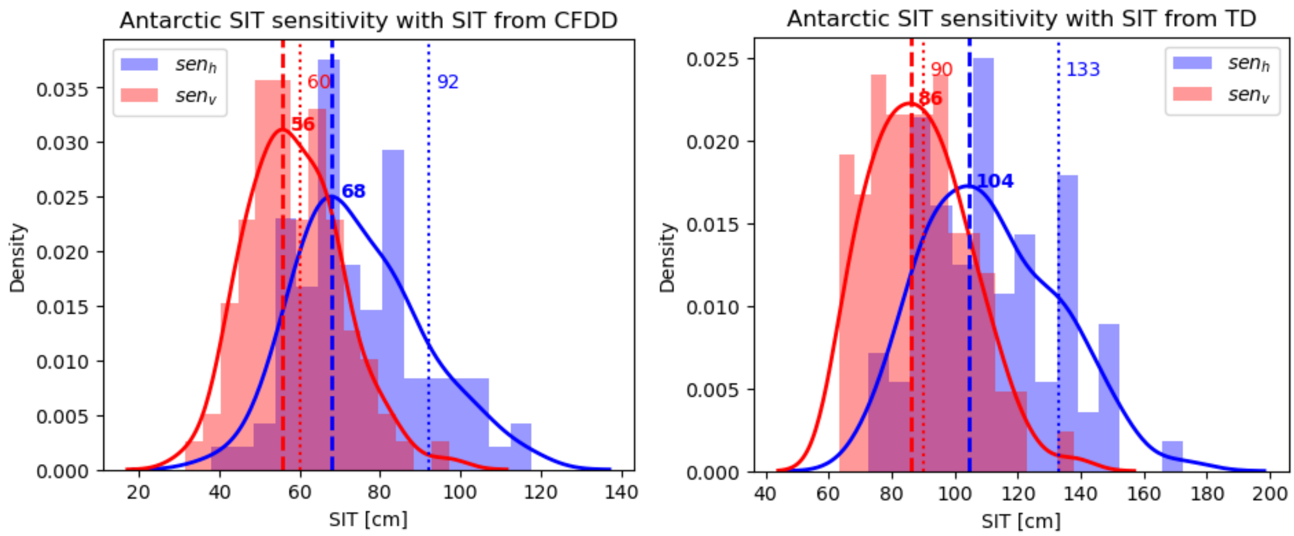

Figure 4.12: Antarctic sensitivity histogram of all runs
Histogram of SIT sensitivities for parameter fits in the Antarctic with SIT from the CFDD model (left) and the TD model (right). Dotted line represents Arctic sensitivity values. Dashed line represents mode of KDE (Kernel density estimation).

4.4 Dependence of snow thickness on TB

The higher B parameter compared to the CIMR ATBD value obtained in my analysis, and its variability, indicate the influence of another physical effect. And since different physical effects contribute to the L-band TB, and snow has a large influence on the TB (Huntemann et al., 2014), I am now investigating the dependence of snow thickness (ST) on TB. I will then try to separate the dependence of ST on TB to obtain fit parameters without the influence of ST. This can make the SIT retrievals more accurate because you can add or subtract a certain amount of TB based on the dependence between ST and TB and how much snowfall has occurred, which you can get from atmospheric data for example, and then retrieve SIT with the reduced TB and fit parameters without the influence of ST.

To get the additional dependence of ST on TB, I use the TD model because it simulates the SIT and ST growth separately. As mentioned before, the TD model probably represents the snowfall in different regions with different atmospheric conditions better than the CFDD model, which assumes 8 % of the SIT as ST. Especially for Antarctica, it will be interesting to see the dependence of ST on TB, as the snowfall in Antarctica is much higher and not well represented by the CFDD model assumption.

Different physical effects contributing to the TB, such as snow thickness, can cause differences in the fit parameters. Snow on top of the ice decreases the difference in permittivity and thus increases the emissivity of sea ice. Therefore, sea ice without any snow cover has lower TBs than sea ice with snow. Both, TB_h and TB_v increase with snow depth at any ice thickness, but the dependence on snow cover is more pronounced for TB_h (Huntemann, 2015).

But first I will look at the snowfall in region D (Baffin Bay) in the Arctic, because for both models the values of parameter B in region D are considerably smaller, with the value of 220 K being about 10 K lower compared to the other regions (see Table 4.1 and 4.2), and are the values closest to the CIMR ATBD values. So perhaps region D and the CIMR ATBD training area are similarly influenced by some other variable such as snowfall. I will look at the snowfall in this region compared to the others, to see differences that may affect the TB and parameter retrieval. Figure 4.13 shows the Arctic ice thicknesses compared to the snow thicknesses for region D in orange and for all other regions in blue. It can be seen that although the ST is not the highest, the ST in region D is not different from the other regions. This alone cannot explain the differences in the B parameters, but a comparison with actual measurements would be desirable.

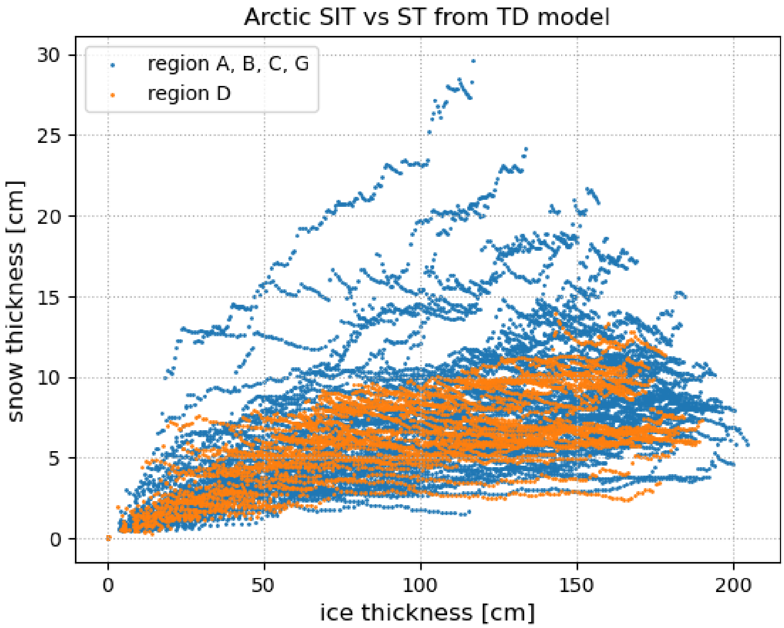

Figure 4.13: Arctic SIT against ST
SIT compared to ST in the Arctic from the TD model. Region D is colored in orange, other regions in blue.

To get a first impression of the dependence of ST on TB, I first visualized the ST as the third variable for all data points in the plot of SIT versus TB_h. Figure 4.14 shows the SIT from the TD model and the horizontal TBs of the Arctic, with the color indicating the snow thickness calculated with the TD model. Figure 4.14 shows that the ST increases with SIT, and only a few data points show a very high ST for SIT less than 50 cm. It can be seen that the highest horizontal TBs are SIT with the highest ST. Although it should be noted that the data points are superimposed on each other, this visualization effect will be removed in the next step by looking separately at the dependence of ST on TB_h at different ice thicknesses. For the Antarctic, Figure 4.15 shows the snow thickness with the dependence of horizontal TB on SIT. Note the different axis for snow thickness in the Arctic and Antarctic. As in the Arctic, Figure 4.15 shows increasing ST with increasing SIT, but the main difference to the Arctic seen in this plot is that the highest ST is seen at lower TB_h for thick sea ice. This could be due to the occurrence of flooding events in the Antarctic, as mentioned earlier. As the snow thickness is much higher in the Antarctic, the pressure can lead to flooding of the ice surface and the formation of snow-ice, which would then reduce the TB.

To obtain a dependence of ST on TB, I create SIT intervals at different ice thicknesses to look at. For the interval, I used ± 1 cm SIT because it removes the dependence of ice thickness on TB. Figure 4.16 shows the dependence of ST on TB at different SIT intervals for the Arctic on the left and for the Antarctic on the right. The circle and triangle indicate TB_h and TB_v, respectively. The color indicates the snow surface temperature. A least squares polynomial fit is performed on the data and the slope of the regression line is described by the number in the legend. For an easier comparison of the scatter of TB_h and TB_v, one can also look at Figure 0.2 in the Appendix. Here, the color indicates only the horizontal and vertical polarization.

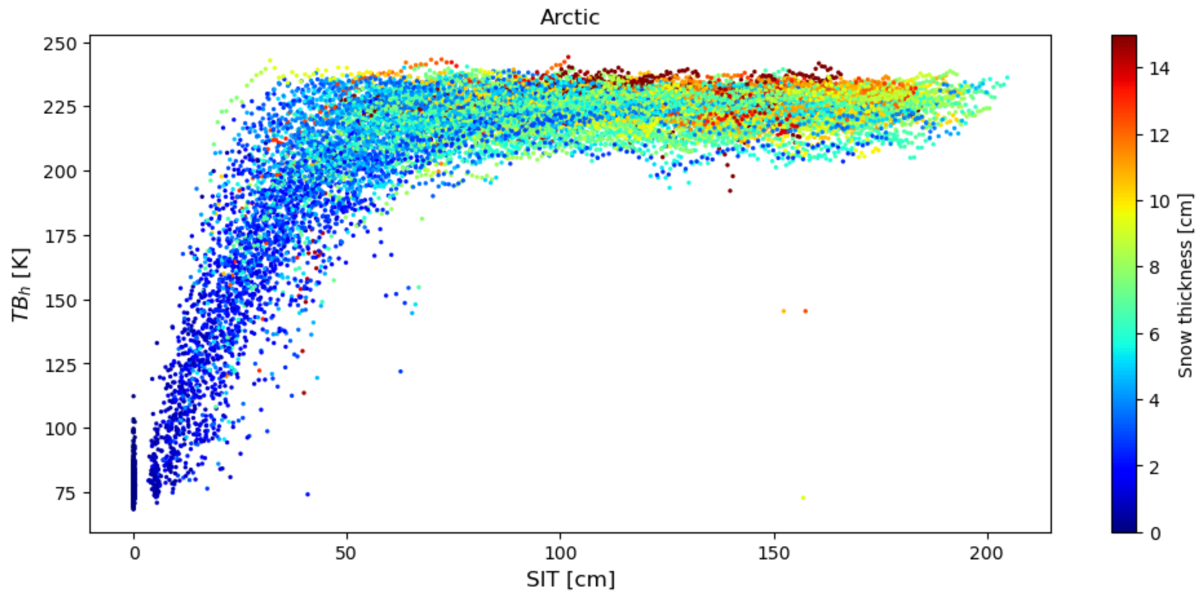

Figure 4.14: Arctic SIT vs TB_h with snow thickness as color
SIT from TD model at all areas from 2011 to 2020 in Arctic against horizontal SMOS TB. Colors indicate snow thickness from TD model.

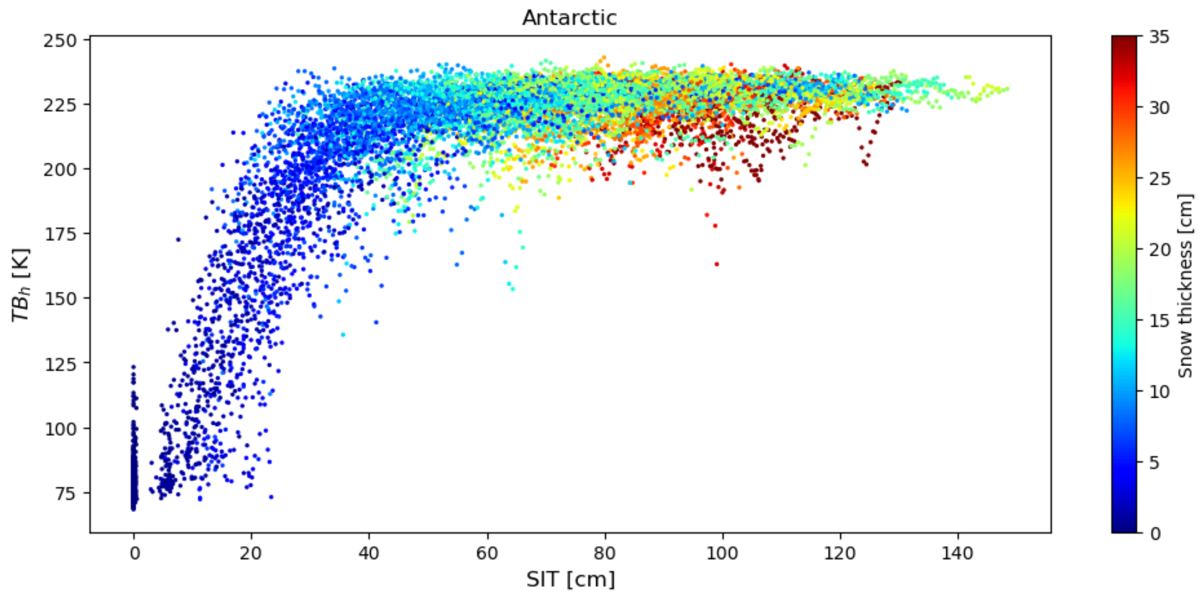

Figure 4.15: Antarctic SIT vs TB_h with snow thickness as color
SIT from TD model at all areas from 2011 to 2021 in Antarctic against horizontal SMOS TB. Colors indicate snow thickness from TD model.

In the Arctic, the dependence or slope of ST on TB_h is greater than on TB_v for almost all SIT intervals, and is strongest at SIT of 30 cm and 50 cm. All intervals show a positive slope, indicating that at this SIT the highest TBs are correlated with the highest snow thicknesses. Although some data points indicate this dependence and the scatter decreases and the correlation becomes clearer at greater ice thicknesses, the overall scatter is large and a clear relation as suggested from Figure 4.14 could not be established. For example, at 30 cm SIT there is certainly no ice that has less than 140 K in TB_h, and probably not less than 160 K. So these would all be outliers affecting the fit. In this context, the fits with snow thickness unfortunately have little meaning if they come from a simple least squares fit. The scatter in the middle of the ice thicknesses is unfortunately also very strong. Manual filtering or changing the way the data are selected for analysis of this dependence will probably be needed to remove outliers.

For the Antarctic, Figure 4.16 shows a slight positive dependence of ST on TB_h and TB_v for thin ice thicknesses, although the scatter is again large. The dependence or slope of ST on TB_h and TB_v becomes negative for sea ice thicknesses greater than 50 cm. For very thick ice of about 100 cm, the negative slope is greatest. With much less scatter at the 100 cm SIT interval, the relation seen in Figure 4.15, and thus the occurrence of flooding events in the Antarctic, can also be seen here.

For both the Arctic and Antarctic, no direct relation between the snow surface temperature and brightness temperature is visible from this plot.

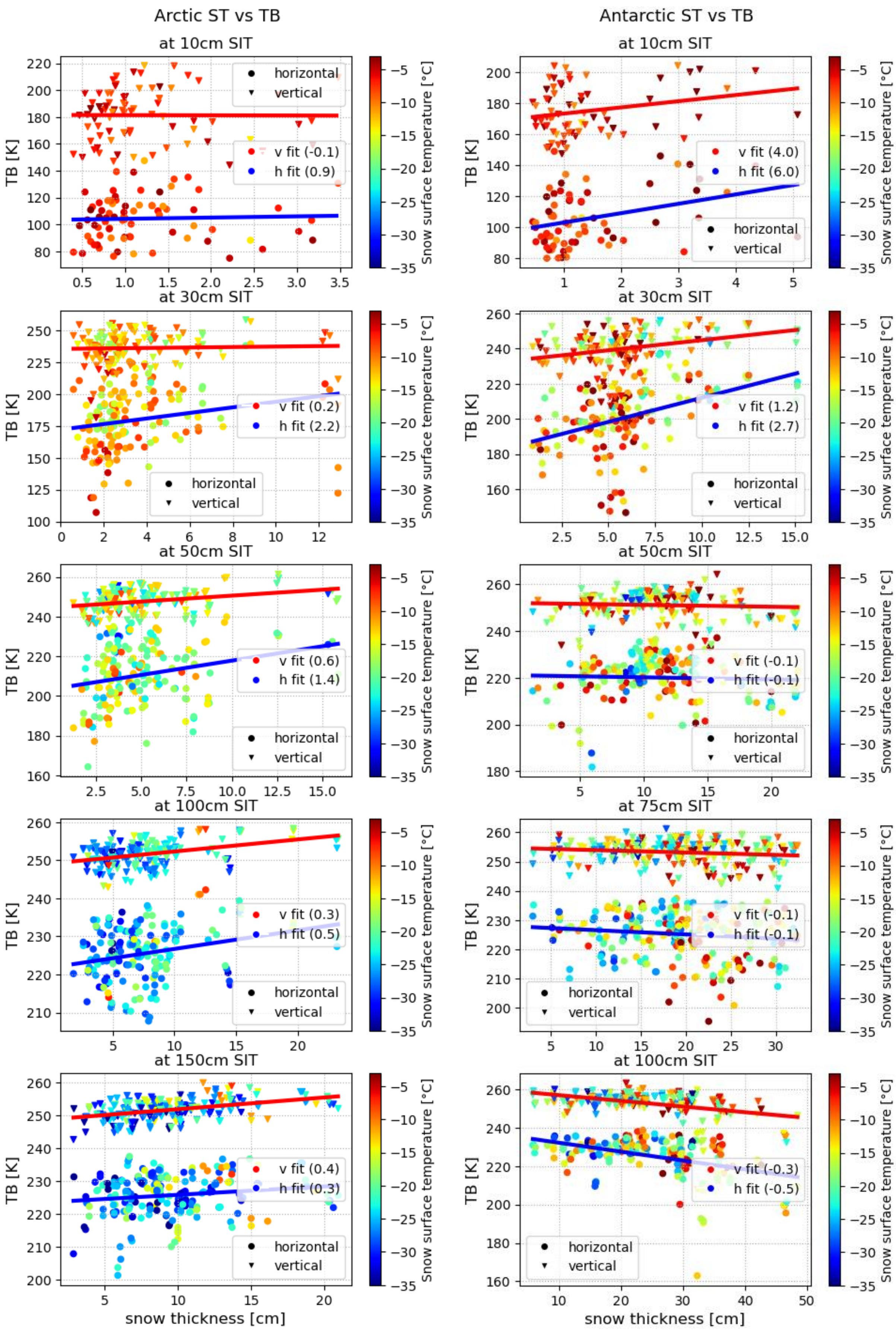

Figure 4.16: ST vs TB for different SIT

ST vs TB for different SIT in the Arctic (left) and in the Antarctic (right). The colors indicate the snow surface temperature and the circle and triangle TB_h *and* TB_v *, respectively. The slope of the regression line is described by the number in the legend.*

5 Summary

The parameter analysis for the Arctic shows, that the parameter values obtained for each freeze up period are scattered around a certain value and that the distributions of the three fitted parameters (A: open water tie point, B: thick sea ice saturation tie point and C: curvature parameter) look almost like Gaussian distributions, which brings the advantage of being able to determine the mean and the standard deviation. The variability in the distributions also assumes that the parameters, and especially B and C, are influenced by other parameters such as snow thickness. Higher variabilities, especially for the parameter B, can be observed for the TB_h fit than for the TB_v fit, caused by the higher variability of TB_h of thick ice.

The parameter A obtained with the modeled SIT from both models does not show differences between the models and is well represented by the CIMR ATBD value, although it shows a slight difference to CIMR ATBD values of 1 K to 2 K (Huntemann & Spreen, 2022). Figure 4.5 and 4.14 shows that small ice thicknesses have the same TBs as open water, which causes the variability in the parameter. The uncertainty could probably be reduced by fine-tuning the starting point of the model more carefully.

The parameter B, on the other hand, does only vary slightly between models, but is about 11 K higher for the TB_h fit and about 5 K higher for the TB_v fit than the CIMR ATBD values. Since TB is influenced by snow, this could explain the variability and difference from the CIMR ATBD values. Another important difference to the CIMR ATBD dataset is the longer time period I analyzed. While only data through December 31 are used for the CIMR ATBD values, I extended the region through April 1, which could potentially affect the saturation of the curve.

The C parameters are lower for the CFDD model than for the TD model. This is mainly caused by the faster ice thickness growth of the TD model, since the same TB is associated with higher ice thicknesses, resulting in a lower curvature fit line and thus a higher C parameter. Both models show differences compared to the CIMR ATBD values. The C parameter with modeled SIT from the CFDD model shows lower than the CIMR ATBD values, which is probably also due to the differences in the B parameters between the datasets, since a higher B parameter results in in a higher curvature fit line and a lower C parameter. Although parameter C can also be influenced by ST, as TB increases with snow depth at any ice thickness (Huntemann, 2015), it is influenced by both parameters A and B, as it connects the two tie points, and thus contains part of their errors and variabilities. In contrast to this, the TD model shows higher values than the CIMR ATBD values, which could be explained by the faster SIT growth than the CFDD model used for the CIMR ATBD values.

For five regions in the Arctic, no significant regional differences were found for parameters A and B in both models, although region D stands out for parameter B with a lower value than the other regions and very similar values to the CIMR ATBD ones. Since snow thickness is a physical effect contributing to the TB, I assumed that this region might not be affected by snowfall as much as other regions. However, this could not be determined as the snow modeled by the TD model does not show significant differences or smaller values compared to other regions. The comparison with actual measurements would be interesting. Parameter C has the largest regional differences, but because of the high variability compared to its value and because it is influenced by many parameters, the regional differences are again negligible.

A slight trend in the parameters can only be seen for the annual means of the C_h parameter for the CFDD model. Parameters A and B show no temporal evolution for any model.

Based on this analysis, the use of regional or annual parameters for the SIT retrieval in the Arctic does not bring any advantage because the variability in each parameter is higher than the regional or annual differences. Assuming that my dataset more accurately represents the TB evolution in the entire Arctic freeze up period, the parameters in Table 5.1 best describe the relation between TB and SIT. These fit parameter values are determined using a single fit for all data of the whole Arctic with SIT from both models separately. Compared to the CIMR ATBD parameters, the newly obtained parameter values show that parameter A could be slightly lower and parameter B could be much higher as expected. The investigation and comparison of which model better simulates the true Arctic ice growth, and which fit parameters, especially the C parameter, should be used to best describe the relation between TB and SIT would be a suggestion for future research, as no measurements are used in this study.

Table 5.1: Fit parameters for one fit of all data in the Arctic
Fit parameters for one fit made of all runs for CFDD and TD modeled ice thicknesses in the Arctic.

parameter	A	B	C
CFDD TB_h	73.8	225.8	17.1
CFDD TB_v	144.8	251.2	10.5
TD TB_h	72.3	227.2	25.7
TD TB_v	144.0	251.8	17.3

The comparison of the Antarctic and Arctic fit parameters shows that parameters A and B are very similar to the Arctic parameter, although the difference in parameter B_v from the Arctic to the Antarctic is much larger than that of parameter B_h. Parameter C shows lower values for the fit with modeled SIT from both models for the Antarctic than for the Arctic. Although the B_h parameter is very similar in the Arctic and Antarctic for both models, the C_h parameter is quite different for both models compared to the Arctic. This suggests that either the relation between TB and SIT is different in Antarctica, more specifically that the relation depends stronger on some other parameter such as snow thickness, or that both models model slower ice thickness growth for the Antarctic than for the Arctic. Furthermore, as with the Arctic parameters, no regional differences in the Antarctic parameters were found. Although region A has lower values for parameter B, and region C has higher values for parameter C than the other two regions. In the Antarctic no significant temporal evolutions are found for parameters A and B, but a strong positive trend is found for parameter C.

Although the parameter retrieval from Antarctica has many uncertainties, I also determined the fit parameters using a single fit to all the data from all of Antarctic for both models under the assumption that they represent the SIT correctly. The parameter values are shown in Table 5.2.

Table 5.2: Fit parameters for one fit of all data in the Antarctic
Fit parameters for one fit made of all runs for CFDD and TD modeled ice thickness in the Antarctic.

parameter	A	B	C
CFDD TB_h	73.6	227.5	12.9
CFDD TB_v	142.6	253.7	10.6
TD TB_h	73.3	230.1	20.8
TD TB_v	142.4	255.0	17.3

The sensitivity analysis showed lower sensitivity values for the fits with SIT from the CFDD model than for the fits with SIT from the TD model. Also the sensitivity values are lower for the fits with SIT from the CFDD model and higher for the fits with SIT from the TD model than the calculated values with the CIMR ATBD parameter. This can be explained by the strong dependence of the sensitivity values to the C parameter, which goes hand in hand with the way sensitivity is determined. The sensitivity in the Arctic with my parameter values from Table 5.1 would be 92.5 cm and 58.2 cm for the CFDD model for the TB_h and the TB_v fits, respectively, and 128.9 cm and 87.4 cm for the TD model for the TB_h and the TB_v fits, respectively.

The sensitivity values in the Antarctic are lower than in the Arctic values for both models and fits, which can again be explained by the lower C parameter in the Antarctic. The sensitivity in Antarctica with my parameter values from Table 5.2 would be 73.6 cm and 59.1 cm for the CFDD model for the for the TB_h and the TB_v fits, respectively, and 109.0 cm and 88.1 cm for the TD model for the TB_h and the TB_v fits, respectively.

6 Discussion and Conclusion

With a long time series of 10 years of SMOS L-band TB data at 53° incidence angle, I have created a new data set to analyze the fit parameters used for the CIMR SIT retrieval algorithm of Huntemann and Spreen (2022). For the parameter retrieval, modeled SIT from the CFDD model (Bilello, 1961) and a modified version of the thermodynamic energy balance model of Tonboe (2005) and Tonboe (2010) are used. In the analysis, the TB evolution is given the least error because of its high accuracy (Wu et al., 2013), although no sea ice drift was assumed, which could cause different TB evolutions. Sea ice drift differs between regions and could be investigated and corrected, for example, with the ice drift product from the Ocean and Sea Ice Satellite Application Facility (OSI-SAF). The modeled SIT probably introduces the largest error, as the difference in ice thickness between the two simple models is large.

The parameter retrieval is based on the relation between TB and SIT. To reduce the variability of this dependence, freeze up runs are selected based on their continuity with ERA5 sea ice concentration data. The selection of continuous sea ice concentration runs is necessary, since both models cannot simulate sea ice thinning, which would lead to a incorrect dependence between TB and SIT and would distort the parameters. The parameter estimation is performed under the assumption that the TBs and the ice thicknesses of both models are correct. Using the analytical Equation (2.4), the fit parameters are obtained empirically for each freeze up run in each region of the Arctic and Antarctic. Again, A is the open water tie point, B is the thick sea ice saturation tie point and C is the curvature parameter.

With more regions used in this data set, no regional differences in either the Arctic or Antarctic can be detected and no advantage of using regional parameters is suggested. However, for the Arctic, significant differences in the parameter distributions of parameter B and C are detected compared to the CIMR ATBD values. The higher values of the B parameter detected with both models of about 11 K for the TB_h fit and about 5 K for the TB_v fit may be due to the longer freeze up period to 1 April used in this analysis compared to 31 December in Huntemann and Spreen (2022), as considering a longer time series of freeze up runs could potentially affect the saturation of the curve and thus the thick sea ice saturation tie point. The variability of this parameter may be influenced by snow, as a slight positive correlation between ST and TB is found for thick ice with the TD model for the Arctic, in agreement with (Huntemann, 2015). Parameter C shows lower values for the CFDD model and higher for the TD model compared to the CIMR ATBD values, due to the different ice growth rate, and is also influenced by both parameters and their variability. Only parameter A is in good overall agreement with CIMR ATBD values. Between the Arctic and Antarctic, only a lower value of the curvature parameter is found in the Antarctic, indicating an earlier saturation of TB.

Another interesting aspect of the analysis is that by separating the parameters for each year, a positive trend in the C parameter can be detected for the Arctic and Antarctic. Under the assumption that the modeled SIT and TB are true, an increase in the curvature parameter represents a later reached saturation, which causes the sensitivity to SIT to be higher. A possible reason for this could be a decrease in the overall salinity of the sea ice over the years, as a less saline ice allows for the retrieval of greater thicknesses (Tian-Kunze et al., 2014). Overall, the sensitivities of TB to changes in SIT are higher for the Arctic than for the Antarctic because the sensitivity is strongly dependent on C, as the degree of curvature affects the slope of the fit function, which is how the sensitivity is determined.

The new retrieved parameter for the whole dataset can be seen for the Arctic and Antarctic in Tables 5.1 and 5.2, respectively. These values suggest that for the Arctic, the current parameter obtained in the CIMR ATBD do not represent the relation between TB and SIT for my data set. The comparison with actual measurements does not make sense, since SIT on the scale of 50km is not easy to determine, and making these kinds of measurements with the accuracy needed to really improve the SIT retrieval would come at an immense cost. However, one could compare the retrieved SIT with the newly determined parameter with other SIT models and discuss which model better represents the Arctic SIT growth. The Antarctic fits may be less reliable because the upper tie point for thick ice is usually not reached, as the fit curve still has a curvature there, and there is more drift, movement, and snowfall in Antarctica. The investigation into Antarctica involves even greater uncertainties, since the SIT evolution is subject to high uncertainties, as we cannot assume that the models represent true SIT values for the Antarctic, since both models can only simulate normal ice growth and do not take into account e.g. flooding. The investigation with different models such as the SNOWPACK (Wever et al., 2020) and ICEPACK (https://github.com/CICE-Consortium/Icepack) models, which include effects such as flooding, would be recommended for future studies.

The investigation of the dependence of snow thickness on TB shows a slight positive correlation of TB with ST in the Arctic, which becomes more reliable due to less scatter at higher ice thicknesses, and a negative correlation at high ice thicknesses in the Antarctic. This means that in the Antarctic lower measured TB at high ice thicknesses could indicate high ST. This observed correlation could indicate flooding as it reduces the TB. Further investigation of the snow dependence on TB and separating it from the fit would lead to more accurate SIT retrievals and could possibly be done in future studies. For this, the inclusion of temperature analysis and a microwave emission model, such as MEMLS (Proksch et al., 2015) or Tonboe (2005) would be beneficial.

7 References

Balsamo, G., Agusti-Panareda, A., Albergel, C., Arduini, G., Beljaars, A., & Bidlot, J., et al. (2018). Satellite and In Situ Observations for Advancing Global Earth Surface Modelling: A Review. *Remote Sensing*, *10*(12), 2038. https://doi.org/10.3390/rs10122038

Bilello, M. A. (1961). Formation, Growth, and Decay of Sea-Ice in the Canadian Arctic Archipelago. *ARCTIC*, *14*(1). https://doi.org/10.14430/arctic3658

Crocker, G. B., & Wadhams, P. (1989). Modelling Antarctic Fast-Ice Growth. *Journal of Glaciology*, *35*(119), 3–8. https://doi.org/10.3189/002214389793701590

Dara Entekhabi, Simon Yueh, Peggy E. O'Neill, Kent H. Kellogg, Angela Allen, & Rajat Bindlish, et al. (2014). SMAP Handbook: Soil Moisture Activer Passive. Mapping Soil Moisture and Freeze/Thaw from Space. Retrieved from https://smap.jpl.nasa.gov/system/internal_resources/details/original/178_SMAP_Handbook_FINAL_1_JULY_2014_Web.pdf

El Hajj, M., Baghdadi, N., Zribi, M., Rodríguez-Fernández, N., Wigneron, J., & Al-Yaari, A., et al. (2018). Evaluation of SMOS, SMAP, ASCAT and Sentinel-1 Soil Moisture Products at Sites in Southwestern France. *Remote Sensing*, *10*(4), 569. https://doi.org/10.3390/rs10040569

ESA. (2012). SMOS (Soil Moisture and Ocean Salinity) Mission. Retrieved from https://www.eoportal.org/satellite-missions/smos. URL last accessed January 25, 2023

ESA. (2017). SMOS Data Products - Brochure. Retrieved from https://earth.esa.int/eogateway/documents/20142/37627/SMOS-Data-Products-Brochure.pdf/9f64eb85-afc9-e48d-0c4e-291d3d710abe

ESA. (2020). CIMR (Copernicus Imaging Microwave Radiometer). Retrieved from https://www.eoportal.org/satellite-missions/cimr. URL last accessed January 17, 2023

ESA. (2023). Copernicus Imaging Microwave Radiometer (CIMR) Mission Requirements Document. Version 5.0. Retrieved from https://cimr.eu/mrd_v5

Gupta, M., Gabarro, C., Turiel, A., Portabella, M., & Martinez, J. (2019). On the retrieval of sea-ice thickness using SMOS polarization differences. *Journal of Glaciology*, *65*(251), 481–493. https://doi.org/10.1017/jog.2019.26

Hersbach, H., Bell, B., Berrisford, P., Biavati, G., Horányi, A., & Muñoz Sabater, J., et al. (2023). ERA5 hourly data on single levels from 1940 to present. Copernicus ERA5 hourly data on single levels from 1940 to present. Climate Change Service (C3S) Climate Data Store (CDS), DOI: 10.24381/cds.adbb2d47.

Hosoda, K. (2010). A review of satellite-based microwave observations of sea surface temperatures. *Journal of Oceanography*, *66*(4), 439–473. https://doi.org/10.1007/s10872-010-0039-3

Huntemann, M. (2015). Thickness retrieval and emissivity modeling of thin sea ice at L-band for SMOS satellite observations (Dissertation, Physik und Elektrotechnik). Universität Bremen, Bremen.

Huntemann, M., Heygster, G., Kaleschke, L., Krumpen, T., Mäkynen, M., & Drusch, M. (2014). Empirical sea ice thickness retrieval during the freeze-up period from SMOS high incident angle observations. *The Cryosphere*, *8*(2), 439–451. https://doi.org/10.5194/tc-8-439-2014

Huntemann, M., & Spreen, G. (2022). CIMR L2 Sea Ice Thickness ATBD v1. Retrieved from https://cimr-algos.github.io/SeaIceThickness_ATBD/intro.html

IPCC (Ed.). (2022). *The Ocean and Cryosphere in a Changing Climate: Special Report of the Intergovernmental Panel on Climate Change*. [H.-O. Pörtner, D. RobertsC., V. Masson-Delmotte, P. Zhai, M. Tignor, E. Poloczanska, K. Mintenbeck, A. Alegría, M. Nicolai, A. Okem, J. Petzold, B. Rama, N.M. Weyer (eds.)]: Cambridge University Press.

Kaleschke, L., Maaß, N., Haas, C., Hendricks, S., Heygster, G., & Tonboe, R. T. (2010). A sea-ice thickness retrieval model for 1.4 GHz radiometry and application to airborne measurements over low salinity sea-ice. *The Cryosphere*, *4*(4), 583–592. https://doi.org/10.5194/tc-4-583-2010

Kaleschke, L., Tian-Kunze, X., Maaß, N., Mäkynen, M., & Drusch, M. (2012). Sea ice thickness retrieval from SMOS brightness temperatures during the Arctic freeze-up period. *Geophysical Research Letters*, *39*(5), n/a-n/a. https://doi.org/10.1029/2012GL050916

Kang, E.-J., Sohn, B.-J., Tonboe, R. T., Dybkjær, G., Holmlund, K., Kim, J.-M., & Liu, C. (2021). Implementation of a 1-D Thermodynamic Model for Simulating the Winter-Time Evolvement of Physical Properties of Snow and Ice Over the Arctic Ocean. *Journal of Advances in Modeling Earth Systems*, *13*(3), 23. https://doi.org/10.1029/2020MS002448

Lindsey, R., & Scott, M. (2022). Climate Change: Arctic sea ice summer minimum. Retrieved from https://www.climate.gov/news-features/understanding-climate/climate-change-arctic-sea-ice-summer-minimum

Maaß, N., Kaleschke, L., Tian–Kunze, X., Mäkynen, M., Drusch, M., & Krumpen, T., et al. (2015). Validation of SMOS sea ice thickness retrieval in the northern Baltic Sea. *Tellus A: Dynamic Meteorology and Oceanography*, *67*(1), 24617. https://doi.org/10.3402/tellusa.v67.24617

Meredith, M., M. Sommerkorn, S. Cassotta, C. Derksen, A. Ekaykin, & A. Hollowed, et al. (2022). Polar Regions. In IPCC (Ed.), *The Ocean and Cryosphere in a Changing Climate: Special Report of the Intergovernmental Panel on Climate Change. [H.-O. Pörtner, D. RobertsC., V. Masson-Delmotte, P. Zhai, M. Tignor, E. Poloczanska, K. Mintenbeck, A. Alegría, M. Nicolai, A. Okem, J. Petzold, B. Rama, N.M. Weyer (eds.)]* (pp. 203–320). Cambridge University Press. https://doi.org/10.1017/9781009157964.005

Parkinson, C. L. (2022). Arctic sea ice coverage from 43 years of satellite passive-microwave observations. *Frontiers in Remote Sensing*, *3*, 13013. https://doi.org/10.3389/frsen.2022.1021781

Paţilea, C., Heygster, G., Huntemann, M., & Spreen, G. (2019). Combined SMAP–SMOS thin sea ice thickness retrieval. *The Cryosphere*, *13*(2), 675–691. https://doi.org/10.5194/tc-13-675-2019

Petrich, C., & Eicken, H. (2009). Growth, Structure and Properties of Sea Ice. In D. N. Thomas & G. S. Dieckmann (Eds.), *Sea Ice* (pp. 23–77). Oxford, UK: Wiley-Blackwell. https://doi.org/10.1002/9781444317145.ch2

Proksch, M., Mätzler, C., Wiesmann, A., Lemmetyinen, J., Schwank, M., Löwe, H., & Schneebeli, M. (2015). MEMLS3&a: Microwave Emission Model of Layered Snowpacks adapted to include backscattering. *Geoscientific Model Development*, *8*(8), 2611–2626. https://doi.org/10.5194/gmd-8-2611-2015

Rees Jones, D. W., & Worster, M. G. (2013). A simple dynamical model for gravity drainage of brine from growing sea ice. *Geophysical Research Letters*, *40*(2), 307–311. https://doi.org/10.1029/2012GL054301

Richter, F., Drusch, M., Kaleschke, L., Maaß, N., Tian-Kunze, X., & Mecklenburg, S. (2018). Arctic sea ice signatures: L-band brightness temperature sensitivity comparison using two radiation transfer models. *The Cryosphere*, *12*(3), 921–933. https://doi.org/10.5194/tc-12-921-2018

Schmitt, A., & Kaleschke, L. (2018). A Consistent Combination of Brightness Temperatures from SMOS and SMAP over Polar Oceans for Sea Ice Applications. *Remote Sensing*, *10*(4), 553. https://doi.org/10.3390/rs10040553

Spreen, G., Kaleschke, L., & Heygster, G. (2008). Sea ice remote sensing using AMSR-E 89-GHz channels. *Journal of Geophysical Research*, *113*(C2), 14485. https://doi.org/10.1029/2005JC003384

Thomas Wagner (18.12.18). *Lecture on atmospheric remote sensing: Passive microwave observations*. Retrieved from http://satellite.mpic.de/pdf_dateien/microwave_2018_2019.pdf

Tian-Kunze, X., Kaleschke, L., Maaß, N., Mäkynen, M., Serra, N., Drusch, M., & Krumpen, T. (2014). SMOS-derived thin sea ice thickness: Algorithm baseline, product specifications and initial verification. *The Cryosphere*, *8*(3), 997–1018. https://doi.org/10.5194/tc-8-997-2014

Tonboe, R. T. (2005). A mass and thermodynamic model for sea ice, Tech. rep., Danish Meteorological Institute.

Tonboe, R. T. (2010). The simulated sea ice thermal microwave emission at window and sounding frequencies. *Tellus A*, *62*(3), 333–344. https://doi.org/10.1111/j.1600-0870.2010.00434.x

Wang, X., Key, J. R., & Liu, Y. (2010). A thermodynamic model for estimating sea and lake ice thickness with optical satellite data. *Journal of Geophysical Research: Oceans*, *115*(C12), 9. https://doi.org/10.1029/2009JC005857

Wever, N., Rossmann, L., Maaß, N., Leonard, K. C., Kaleschke, L., Nicolaus, M., & Lehning, M. (2020). Version 1 of a sea ice module for the physics-based, detailed, multi-layer SNOWPACK model. *Geoscientific Model Development*, *13*(1), 99–119. https://doi.org/10.5194/gmd-13-99-2020

Wu, L., Torres, F., Corbella, I., Duffo, N., Duran, I., & Vall-llossera, M., et al. (2013). Radiometric Performance of SMOS Full Polarimetric Imaging. *IEEE Geoscience and Remote Sensing Letters*, *10*(6), 1454–1458. https://doi.org/10.1109/LGRS.2013.2260128

Yang, Q., Losa, S. N., Losch, M., Tian-Kunze, X., Nerger, L., & Liu, J., et al. (2014). Assimilating SMOS sea ice thickness into a coupled ice-ocean model using a local SEIK filter. *Journal of Geophysical Research: Oceans*, *119*(10), 6680–6692. https://doi.org/10.1002/2014JC009963

Appendix

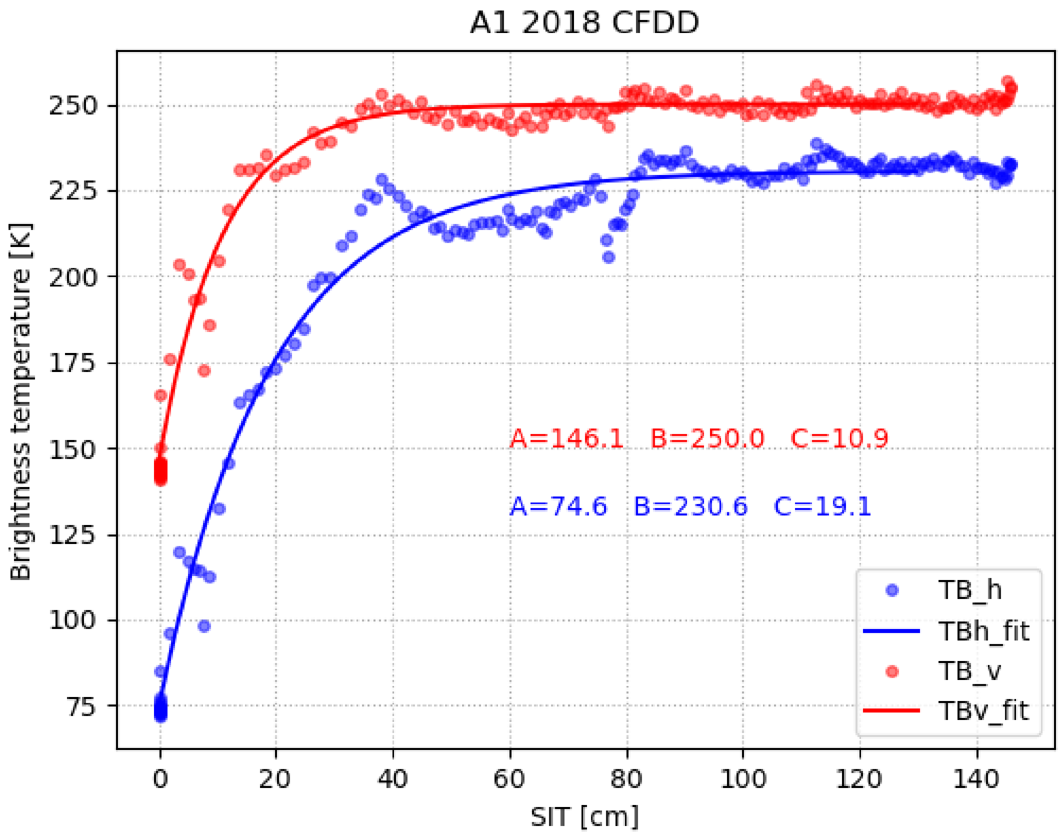

Figure 0.1: Fit curve of area A1 in the Arctic in 2018
Fit curve of area A1 in the Arctic in 2018 with modeled SIT from the CFDD model and SMOS brightness temperatures. The numbers denote the fit parameters and the colors indicate the horizontal (blue) and vertical (red) fit.

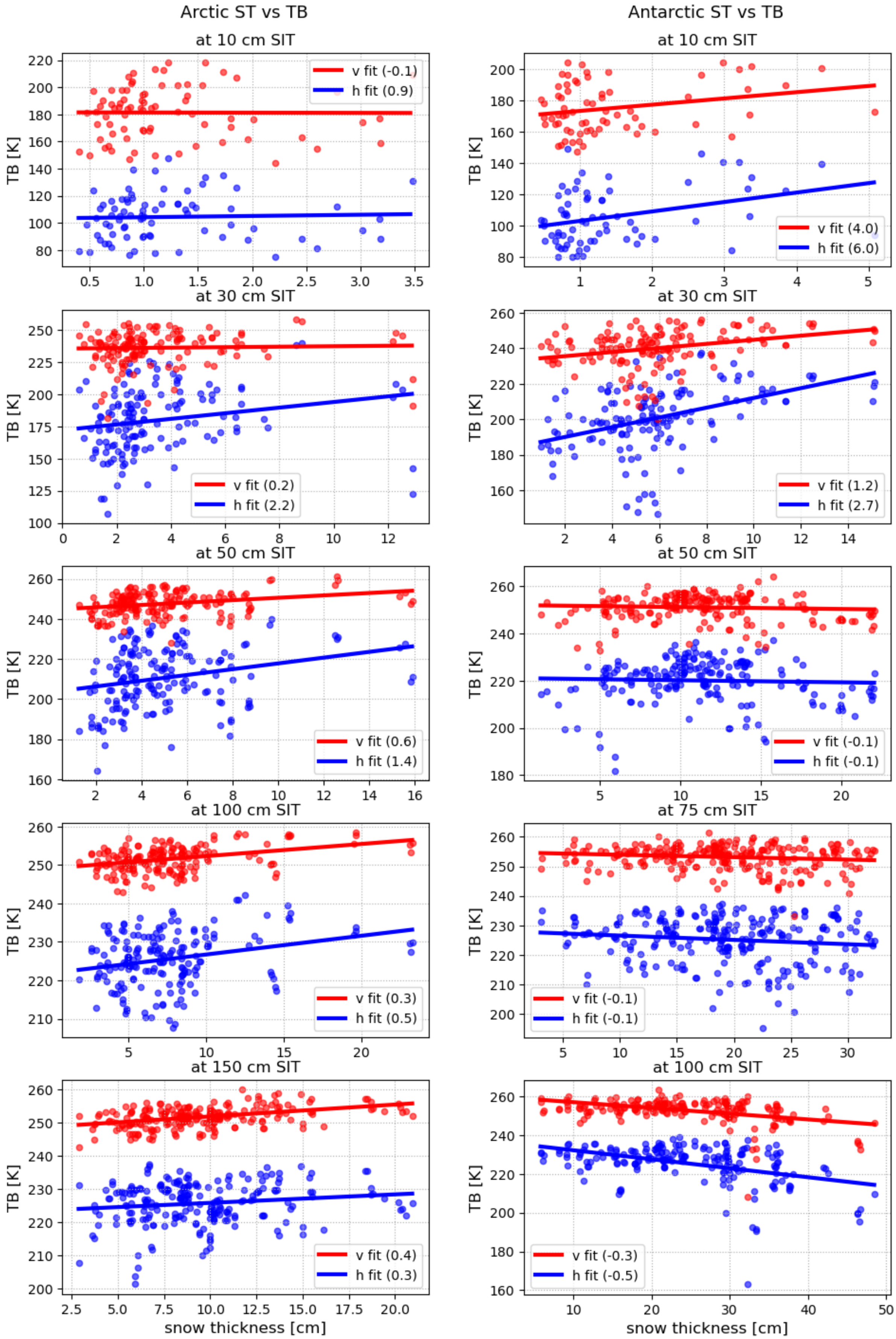

Figure 0.2: ST vs TB for different SIT
ST vs TB for different SIT in the Arctic (left) and in the Antarctic (right). The colors indicate TB_h (blue) and TB_v (red), respectively. The slope of the regression line is described by the number in the legend.

Declaration

I confirm that the master thesis Modelling and Retrieval of Sea Ice Thickness from Microwave Radiometer Satellite Observations is the result of my own work. No other person's work has been used without acknowledgement in the main text of this thesis. This thesis has not been submitted for the award of any other degree or thesis in any other institution.

All sentences or passages quoted in this thesis from other people's work have been specifically acknowledged by clear cross-referencing to author, work and pages. Any illustrations which are not the work of the author of this thesis are specifically acknowledged.

The submitted written version of the thesis corresponds to the version on the electronic storage device (filename: Heilingbrunner_1108877).

____